

R-spondin 3 deletion induces Erk phosphorylation to enhance Wnt signaling and promote bone formation in the appendicular skeleton

Kenichi Nagano¹, Kei Yamana¹, Hiroaki Saito¹, Riku Kiviranta¹, Ana Clara Pedroni¹, Dhairya Raval¹, Christof Niehrs^{2,3}, Francesca Gori^{1*} and Roland Baron^{1,4,5*}.

¹Division of Bone and Mineral Research, Harvard School of Dental Medicine and Harvard Medical School, ²Division of Molecular Embryology, DKFZ-ZMBH Alliance, Deutsches Krebsforschungszentrum (DKFZ), 69120, Heidelberg, Germany, ³ Institute of Molecular Biology (IMB), 55128, Mainz, Germany, ⁴ Department of Medicine Harvard Medical School, ⁵ Endocrine Unit, Massachusetts General Hospital.

*Co-senior Authors

Key Words: R-spondin 3, skeletal homeostasis, Erk signaling, Wnt signaling.

Address correspondence to:

Francesca Gori
Division of Bone and Mineral Research
Department of Oral Medicine, Infection and Immunity
Harvard School of Dental Medicine
Boston, MA 02115
Tel: (617) 432-1940
Email: francesca_gori@hsdm.harvard.edu

And

Roland Baron
Department of Medicine
Harvard Medical School
Boston, MA 02115
Tel: (203) 640-3536
Email: roland_baron@hms.harvard.edu

33

34 **Abstract**

35 Activation of Wnt signaling leads to high bone density. The R-spondin family of four secreted
36 glycoproteins (Rspo1-4) amplifies Wnt signaling. In humans, RSPO3 variants are strongly associated
37 with bone density. Here we investigated the role of Rspo3 in skeletal homeostasis in mice. Using a
38 comprehensive set of mouse genetic and mechanistic studies, we show that in the appendicular
39 skeleton, *Rspo3* haplo-insufficiency and *Rspo3* targeted deletion in *Runx2*⁺ osteoprogenitors lead to
40 an increase in trabecular bone mass, with increased number of osteoblasts and bone formation. In
41 contrast and highlighting the complexity of Wnt signaling in the regulation of skeletal homeostasis, we
42 show that *Rspo3* deletion in osteoprogenitors results in the opposite phenotype in the axial skeleton,
43 i.e., low vertebral trabecular bone mass. Mechanistically, *Rspo3* deficiency impairs the inhibitory
44 effect of Dkk1 on Wnt signaling activation and bone mass. We demonstrate that *Rspo3* deficiency
45 leads to activation of Erk signaling which in turn, stabilizes β -catenin and Wnt signaling activation.
46 Our data demonstrate that *Rspo3* haplo-insufficiency/deficiency boosts canonical Wnt signaling by
47 activating Erk signaling, to favor osteoblastogenesis, bone formation and bone mass.

48 **Introduction**

49 The Wnt signaling pathway controls cell fate decisions and tissue homeostasis during
50 development and in the adult ^{1, 2}. It is also involved in skeletal development and essential for the
51 regulation of bone mass in the adult skeleton ³⁻⁵. Genetic or therapeutic activation of canonical Wnt
52 signaling is associated with increased bone mass ³ and current therapeutic approaches aim at
53 activating this pathway in patients with osteoporosis or osteogenesis imperfecta for instance ⁶.

54 Wnt signaling involves a large number of receptors and co-receptors, and of endogenous agonists
55 and antagonists that, together, tightly regulate its activation ¹⁻⁴. Due to this complexity, and even
56 though Wnt signaling has been studied extensively in recent years in bone, several aspects of the
57 mechanisms by which it regulates bone mass remain unclear. Similarly, the specific downstream

events regulated by the various components of the Wnt signaling machinery and their interaction with other signaling cascades remain puzzling.

In this context, the fact that several studies have demonstrated that the four Roof plate-specific spondin, R-spondins (Rspo1 to 4), synergize with Wnt ligands to activate Wnt signaling^{4, 7-13} raises the question of their potential role in skeletal development and homeostasis. This enhancement of Wnt activity is attributed to the ability of Rspos to prevent the ubiquitination and degradation of the Lrp5/6/Fzd receptor complex via Lgr4-6, closely related orphans of the leucine-rich repeat containing G protein-coupled receptors, and the transmembrane E3 ubiquitin ligases ring finger 43 (Rnf43) and zinc and ring finger 3 (Znrf3), sensitizing cells to Wnt ligands^{7, 14-18}. Although the role of Lgr receptors in the effects of Rspos is well established, recent reports have shown that Rspo2 and Rspo3 can also enhance Wnt signaling independently of Lgr receptors, possibly by acting as direct antagonist ligands to RNF43 and ZNRF3^{11, 19, 20}.

Of particular interest is the fact that, in contrast to the many studies that have reported that Rspos co-activate Wnt signaling, studies in Zebrafish have indicated that Rspo3 can also function as a negative regulator of canonical Wnt signaling during dorsoventral and anteroposterior patterning^{21, 22}. Additionally, it has been shown that Rspos can potentiate non-canonical Wnt cascades, such as the Wnt/PCP signaling^{14, 15} and can function as antagonists of BMPR1 in *Xenopus*²³, two events that could have a negative impact on bone formation and bone mass. Thus, the mechanisms involved in the Rspos/Wnt signaling axis and their influence on skeletal homeostasis appear to be more complex *in vivo*.

The four Rspos belong to a family of cysteine-rich secreted glycoproteins with high structural similarity and 60% sequence homology^{8, 11}. Although all Rspos are expressed in bone during development, they have specific and unique functions as reflected by the findings that their deletion leads to different phenotypes^{10, 13, 24-31}. Within the Rspo family, Rspo3 is of particular interest for bone because it is highly expressed in skeletal elements during mouse development^{32, 33} and

several human GWAS studies have shown that RSPO3 SNPs are strongly associated with bone mineral density and risk of fracture³⁴⁻⁴⁰. Not surprisingly, *in vitro* studies have shown that overexpression of, or treatment with, Rsp3 can enhance Wnt-ligand mediated osteoblast (OB) differentiation^{10, 28, 41}. However, similar to the Zebrafish and *Xenopus* studies mentioned above, it has also been reported that Rspo3 may function as a negative regulator of osteoblast differentiation *in vitro*⁴². Thus, taking into account the entire literature raises questions about the true net influence of Rsp3, and in particular Rspo3, on skeletal homeostasis. We have recently reported that *Rspo3* is expressed in osteoprogenitors in the craniofacial complex in both mice and Zebrafish³³. However, *Rspo3* disruption in Zebrafish has only mild effects on larval craniofacial cartilage skeleton³³ and in mice its haplo-insufficiency does not appear to affect craniofacial development. Nilsson *et al.* have recently reported that targeted deletion of *Rspo3* in osteoblast precursors in mice leads to low bone mass in the axial skeleton (L5) at 12 weeks of age, they examined only the axial skeleton where no changes in cellular and dynamic parameters were observed⁽⁴⁰⁾.

In the current studies, we have further investigated the role of Rspo3 in skeletal homeostasis. We found that if, as recently reported^{40, 43}, targeted deletion of *Rspo3* in Runx2⁺ cells decreases bone mass in the axial skeleton, both global *Rspo3* haplo-insufficiency and targeted deletion of *Rspo3* in Runx2⁺ osteoblast precursors lead to a marked increase in trabecular bone mass in the appendicular skeleton in both male and female mice, mainly as a result of increased bone formation. Mechanistically, we found that Rspo3 deletion leads to increased Erk phosphorylation, and, similar to increased Rspo3, stabilization of β -catenin and, activation of Wnt signaling, revealing a novel Rspo3/Erk/Wnt signaling axis that contributes to the regulation of skeletal homeostasis.

Results

***Rspo3* haplo-insufficiency increases bone formation and trabecular bone mass**

Rspo3 is expressed in bone during mouse skeletal development³². We assessed *Rspo3* mRNA levels in primary calvarial osteoblasts (cOBs) and found that it is expressed in these cells and that its

expression increases significantly during OB differentiation (Figure 1- figure 1 supplement 1a). To determine the physiological role of *Rspo3* in skeletal homeostasis, we first used mice in which *Rspo3* has been germline-deleted²⁷. As global deletion of *Rspo3* leads to lethality by E9.5^{24, 27}, before skeletal development, we analyzed mice lacking only one *Rspo3* allele (*Rspo3*^{+/-}) and their WT littermates. *Rspo3*^{+/-} mice are born at the expected Mendelian ratio and their axial and appendicular skeleton develop normally (Figure 1- figure supplement 1b). *Rspo3*^{+/-} mice continue to be healthy and do not develop any detectable pathology as they age (up to one year) (data not shown). We confirmed that *Rspo3* mRNA levels were significantly decreased (50%) in *Rspo3*^{+/-} mice in both marrow-depleted long bones and in cultured cOBs compared to WT mice (Figure 1a and Figure 1- figure supplement 1a). Contrary to expectations, Two-Way ANOVA analysis of the skeletal phenotype at 6-, 12- and 18-wk of age (Figure 1b, Table 1, Figure 1 - figure supplement 1c, Table S1), revealed highly significant (p<0.001) anabolic effects of *Rspo3* haplo-insufficiency on structural, cellular, and dynamic parameters in both female and male mice. The skeletal phenotype of *Rspo3*^{+/-} male and female mice is overall characterized by an increase in trabecular bone mass with high bone formation, mineral apposition rate and OB number and surface whereas bone resorption parameters are not affected, as indicated by osteoclast (OC) number and surface as well as eroded surface (ES/BS) (Figure1b, Table 1, Table S1).

As expected, Two-Way ANOVA also demonstrated an effect of age, affecting primarily the structural parameters (Figure 1b, Table 1 and Table S1). At 12-wk of age *Rspo3* haplo-insufficiency led to a significant increase in trabecular bone mass (BV/TV), trabecular thickness (Tb.Th.) and trabecular number (Tb.N) (Fig. 1 c-d, Table 1 and Table S1). Trabecular bone resorption parameters (Oc.S/B.Pm and N.Oc/B.Pm) were not changed in both *Rspo3*^{+/-} male and female mice. In contrast, *Rspo3*^{+/-} mice exhibited an increase in trabecular bone formation parameters (BFR/BS) (Figure 1d-e, Table 1 and Table S1). This increase in BFR was associated with an increase in mineral apposition rate (MAR), indicating a marked increase in the activity of individual OBs in *Rspo3*^{+/-} mice, in addition

to the increase in their numbers (N.Ob/B.pm, Figure 1d, Table 1 and Table S1). Consistent with these results, the osteoid surface (OS/BS) and the OB surface (Ob.S/B.Pm) were also significantly increased in both sexes (Table 1 and Table S1). Despite these marked effects on trabecular bone, cortical bone parameters were not significantly changed in *Rspo3*^{+/-} female and male mice at 12-wk of age (Figure 1d, Table S2 and S3). In contrast to the observed effects in the tibia, no significant differences in bone mass or cellular activities were noted in the vertebrae (L5) at 12-wk of age (Figure 1- figure supplement 2 and Table S4), indicating that *Rspo3* haplo-insufficiency affects preferentially the trabecular bone compartment in long bones.

Thus, in contrast with the expectation that decreasing the expression of a Wnt signaling potentiator might lead to a decrease in bone mass, our data clearly indicates that in the appendicular skeleton *Rspo3* haplo-insufficiency induces an increase in trabecular bone mass due to a significant increase in bone formation, with no changes in bone resorption in both males and females. In agreement with our *in vivo* observations, we found that, although *Rspo3* is expressed in bone marrow macrophage (BMM)-derived OCs (Figure 1- figure supplement 3a), there was no significant differences in the formation of TRAP⁺ multinucleated cells and in the expression of OC marker genes (*Ctsk*, *Trap*, *Nfatc1*) between BMM cultures from WT and *Rspo3*^{+/-} mice in response to M-CSF and RANKL (Figure 1- figure supplement 3b and 3c). In addition, mix-and-matched co-cultures of cOBs and BMMs from WT or *Rspo3*^{+/-} mice confirmed that *Rspo3* haplo-insufficiency does not affect osteoclastogenesis, whether directly or indirectly (Figure 1- figure supplement 3d).

***Rspo3* haplo-insufficiency leads to an increase in bone marrow precursor cells and in their osteoblast potential**

Given that the OB number was significantly increased in *Rspo3*^{+/-} mice compared to WT mice (Figure 1, Table 1 and Table S1) we determined whether this was associated with an increase in the population of precursor cells. Bone marrow flow cytometry showed that while the total number of bone stromal cells (Lin⁻CD45⁻) was not significantly affected by *Rspo3* haplo-insufficiency (4047±1245 in

WT compared to 5867+2382 in *Rspo3*^{+/-}, mean±SEM n=10), the mesenchymal stromal cells (MSC) population (defined here as Lin⁻CD45⁻CD31⁻CD51⁺Sca-1⁺)⁴⁴ was significantly increased in *Rspo3*^{+/-} mice compared to WT littermates (p=0.015) (Figure 2a and 2b). Consistent with these findings and with the observed increase in OB number and bone formation, *Rspo3* haplo-insufficiency significantly increased CFU-F (p=0.04) and CFU-OB (p=0.034) formation (Figure 2c). Importantly, while treatment with recombinant *Rspo3* did not affect CFU-F and CFU-OB potential of WT BMSCs, it showed a tendency to decrease CFU-F and rescued significantly, i.e., prevented, the *Rspo3* haplo-insufficiency-dependent increase in CFU-OB formation (Figure 2c). These data show that the changes induced by *Rspo3* haplo-insufficiency cell-autonomously affect the bone marrow MSC lineage and induce an increase in the pool of progenitor cells with OB potential.

Specific deletion of *Rspo3* in *Runx2*⁺ cells leads to high bone mass in the appendicular skeleton and low bone mass in the axial skeleton

To confirm the cell-autonomous effect of *Rspo3* to cells of the OB lineage *in vivo*, we generated mice with deletion of *Rspo3* in the OB lineage (*Rspo3*-OB-cKO) by crossing *Rspo3*^{fl/fl} mice with the OB progenitors-specific *Runx2-Cre* mice^{45, 46}. OB lineage-targeted deletion of *Rspo3* (Figure. 3a) reproduced the skeletal phenotype seen in the appendicular skeleton of *Rspo3*^{+/-} mice as indicated by a significant increase in BV/TV (females p=0.017, males p<0.0001), MAR (females p=0.0034, males p<0.0001), BFR/BS (females p=0.0012, males p<0.0001) and N.Ob/B.Pm (p=0.033, males p= 0.007) in *Rspo3*-OB-cKO compared to their control (*Rspo3*^{fl/fl}) littermates. Once again there were no changes in OC parameters (Table S5). μ CT analysis of the femur, confirmed a significant increase in BV/TV, Tb.N, and Conn.D in both males and females (Figure 3d).

Very surprisingly however, and although the basal expression level of *Rspo3* and the efficiency of deletion in long bones and vertebrae was similar (Figure 3a and Figure 4a), L5 μ CT analysis showed a significant decrease in BV/TV, Tb.N, Tb.Th and Conn.D accompanied by a marked increase in Tb.Sp. and SMI in *Rspo3*-OB-cKO compared to their control (*Rspo3*^{fl/fl}) male and female littermates

(Figure 4b), confirming a recent report ⁴³. Bone histomorphometry analysis showed that structural parameters were also significantly decreased but only in *Rspo3*-OB-cKO males compared to the control group (Figure 4c-d and Table S6). No significant changes were seen in the dynamic parameters. While the N.Ob/B.Pm and Ob.S/BS were not changed, the N.Oc/ B.Pm was significantly increased in *Rspo3*-OB-cKO males but not females, compared to the control group (Figure 4d and Table S6), providing a possible explanation for the decreased bone mass, at least in males. Thus, our studies show that targeted deletion of *Rspo3* in *Runx2*⁺ osteoprogenitors leads to an opposite bone phenotype in the appendicular and the axial skeleton. Excluding any effect of the transgene or the floxed allele on the differential effect of *Rspo3* targeted deletion in the axial and appendicular skeleton, μ CT analysis of the femur and L5 vertebrae did not show any structural difference in BV/TV, Tb.N, Tb.Th or Tb.Sp between *Runx2-Cre*, WT and *Rspo3*^{f/f} mice (Figure 3 and 4- figure supplement 1).

***Rspo3* haplo-insufficiency and deletion lead to β -catenin stabilization**

Independent of the differences, at least at the 12-wk time point, between axial and appendicular skeletal sites, our results showed a clear increase in OB progenitors in the bone marrow of *Rspo3*^{+/-} mice (Figure 2) and given that trabecular bone is the main compartment affected by *Rspo3* haplo-insufficiency, we then explored how depletion of *Rspo3* was affecting Wnt signaling in BMSCs. Surprisingly, but consistent with our observations on bone formation, *Rspo3* haplo-insufficiency led to a remarkable increase in the expression of known canonical Wnt target genes *Axin2* and *Tcf7* and increased active β -catenin levels (Figure 5a and 5b). In addition, *Runx2* expression was also significantly increased in *Rspo3*^{+/-} BMSCs (Figure 5a). In addition, *Rspo3* haplo-insufficiency led to a significant increase in the expression of *Axin2* and *Dkk1*, but not *Sost* in marrow depleted long bone cortical bone (Figure 5c). Thus, surprisingly but consistent with the bone and OB phenotypes, *Rspo3* haplo-insufficiency leads to activation of canonical Wnt signaling.

To exclude any function of the remaining *Rspo3* on canonical Wnt signaling in the *Rspo3*^{+/-} mice and cells, we generated *Rspo3*^{-/-} mouse embryonic fibroblasts (MEFs) at E9.5, before embryonic lethality^{24, 27}. As shown by several groups^{7, 8, 12, 29}, we confirmed that while *Rspo3* does not activate Wnt signaling by itself, it potentiates exogenous Wnt3a action in WT MEFs as indicated by the Tcf7/Lef luciferase reporter assay (Figure 6 - figure supplement 1a). However, and similarly to what is observed in *Rspo3* haplo-insufficient BMSCs and bone marrow depleted long bones cortical bone, at steady-state *Rspo3* deficiency (p<0.0001) (Figure 6 - figure supplement 1b) led to a marked increase in the expression of the canonical Wnt target genes *Tcf7* (p<0.0001) and *Axin2* (p=0.0017) as well as to a significant increase in the levels of phosphorylated Lrp6 (pLrp6), activated β -catenin and Tcf1 (Figure 6a and 6b). Accordingly, at steady state TOPflash reporter activity was significantly higher in *Rspo3* null MEFs compared to WT MEFs (Figure 6a). Upon Wnt3a treatment, as expected, *Axin2* and *Tcf7* gene expression as well as pLrp6, activated β -catenin levels and TOPflash reporter activity were increased in WT MEFs but were significantly higher in *Rspo3* null MEFs (Figure 6a and 6b). Thus, haplo-insufficiency and absence of *Rspo3* in BMSCs and MEFs led to β -catenin stabilization and enhancement of β -catenin-dependent signaling. We then explored the mechanisms by which this might occur.

***Rspo3* haplo-insufficiency and deletion impair Dkk1-Wnt inhibitory activity**

Activation of canonical Wnt signaling results from changes in endogenous activators and/or inhibitors levels and/or their activity. Interestingly, we found that Wnt3a significantly decreased the expression of *Rspo3* in WT MEFs, whereas it is significantly increased by Dkk1 (Figure 7a). Based on our results with *Rspo3*^{+/-} and *Rspo3*^{-/-} cells, this raised the possibility that *Rspo3* participates in a feedback loop that tones down canonical Wnt activity. As shown in Figure 7b, we found that the ability of Dkk1 to block Wnt3a-dependent activation of canonical Wnt signaling was significantly impaired in the absence of *Rspo3*: whereas in WT MEFs 50% reduction in the reporter activity was achieved by 50 ng/mL Dkk1, a dose of 400 ng/mL Dkk1 (8x higher) was needed to obtain the same level of

inhibition in *Rspo3* null MEFs (Figure 7b). Impairment of Dkk1 efficacy in *Rspo3* null MEFs was also confirmed by pLrp6 and β -catenin protein levels (Figure 7c). To determine whether this relationship between *Rspo3* levels and Dkk1 efficacy was also happening *in vivo*, we crossed *Rspo3*^{+/-} mice with mice expressing high levels of Dkk1 in OBs (*Dkk1-Tg* mice), which exhibit impaired canonical Wnt signaling and low trabecular bone mass due to decreased bone formation^{47, 48}. Supporting our *in vitro* data, *Rspo3* haplo-insufficiency counteracted the negative effect of OB-targeted overexpression of Dkk1 on trabecular bone mass (Figure 7d and 7e and Table S7).

***Rspo3* deletion enhances Erk signaling to increase pLrp6 and stabilize β -catenin**

Since both *Rspo3* haplo-insufficiency and its deletion led to β -catenin stabilization, we asked whether *Rspo3* might regulate other signaling pathways which in turn can stabilize β -catenin, stimulating osteoblastogenesis and counteracting Dkk1 efficacy. It has been proposed that *Rspo3* binding to *Lgr4* inhibits Erk phosphorylation (pErk)^{23, 42, 49}. We therefore investigated whether Erk signaling, known to activate Wnt signaling and to regulate OB differentiation and bone mass⁵⁰⁻⁵³, was affected by the absence of *Rspo3* in MEFs. *Rspo3* deficiency led to a clear and significant increase in pErk basal levels (Figure 8a). Inhibition of pErk by the specific Erk inhibitor U0126, in *Rspo3*^{+/-} cells led to a significant decrease in active β -catenin levels in both steady state and Wnt3a-stimulated cultures. A similar effect was also seen for the levels of pLrp6 (Figure 8a). Confirming these findings, the increase in the expression of the canonical Wnt signaling target genes *Tcf7* and *Axin2* in *Rspo3* null MEFs was also partially rescued by blocking Erk signaling (Figure 8b). In contrast, the Erk inhibitor U0126 significantly decreased both the basal and the Wnt3a-dependent increase in pErk in WT cells but failed to affect significantly active β -catenin levels. Thus, the stabilization of β -catenin seen in the absence of *Rspo3* is due, at least in part, to activation of the Erk pathway.

Consistent with these findings, the increase in CFU-F and CFU-OB formation seen in *Rspo3*^{+/-} BMSCs was significantly decreased by blocking Erk signaling (Figure 9). Not surprisingly, knowing

the role of Erk signaling activation in osteoblastogenesis, a significant decrease in CFU-OB, but not in CFU-F, formation was also seen in WT cells treated with U0126 (Figure 9).

Discussion

Wnt signaling is central to skeletal development and homeostasis in health and disease³. Understanding the biological mechanisms by which this signal operates is therefore of both scientific and clinical interest. R-Spondins, classically considered as positive modulators of Wnt signaling, play an important role in normal development of several tissues and organs, including bone, and are implicated in human diseases^{8, 9, 11-13}. Among the 4 R-Spondins, GWAS studies in humans have shown that RSPO3 might be specifically involved in bone homeostasis due to the strong association between RSPO3 common variants and bone mineral density and fracture rate^{34, 35, 37-39, 43}. Our results demonstrate, through several independent lines of genetic *in vivo* and *in vitro* experiments, that, counter-intuitively, decreasing *Rspo3* levels globally or specifically in *Runx2*⁺ OB precursors leads to increased trabecular bone formation and high bone mass in the appendicular skeleton, mainly driven by increased number of OB progenitors and OBs as well as an increase in their bone forming activity. Unexpectedly though, and as recently reported by Nilsson *et al.*⁴⁰, we also found that while the axial skeleton is only moderately affected in the haplo-insufficient mice, vertebrae are affected in the opposite manner, i.e. with a decrease in trabecular bone mass, after OB precursor-targeted deletion of *Rspo3*. Although it is not possible to identify the mechanism(s) responsible for these differential responses of the skeleton, it is worth mentioning here that axial and appendicular skeleton have different embryonic origin (paraxial mesoderm and later plate mesoderm, respectively)⁵⁴ and that a new population of skeletal stem cells has been recently identified in the vertebrae (vSSC) that is absent from the long bones⁵⁵, raising the possibility that distinct populations of stem cells and non-stem progenitors in the vertebrae and in the long bones might respond differentially to stimuli. These findings underline the complexity of Wnt signaling regulation of bone homeostasis and support the hypothesis that different bone microenvironments, their embryonic origin, their differential

exposure and response to mechanical cues, and the differential expression levels of receptors and co-receptors as well as of agonists and antagonists that balance Wnt signaling activity, might induce specific and distinct skeletal responses. Nevertheless, our findings show that skeletal phenotypes should always be investigated in both the appendicular and axial skeleton, as these two regions may respond differently. In contrast, Nilsson *et al.* performed their studies only in vertebrae. Furthermore, this is a trabecular bone-rich skeletal site, but the DEXA studies that led to the identification of a link between RSPO3 variants and bone fragility in humans were performed in the distal forearm, a cortical-rich appendicular skeletal site^{40, 43}. Furthermore, both groups found that cortical bone is not significantly affected by *Rspo3* haplo-insufficiency or deletion in mice, confirming that trabecular and cortical bone are differentially regulated^{46, 56} and further underlining the biologic complexity of Wnt signaling regulation of bone homeostasis.

Thus, our studies reveal a novel and unexpected role of *Rspo3* in the Wnt signaling machinery and bone homeostasis. Given the unexpected nature of our observations it is important to summarize here the multiple independent *in vivo* and *in vitro* experiments that unequivocally support the novel concept that decreasing the levels of *Rspo3* can, at least *in vitro* and in the cellular environment of the appendicular skeleton's trabecular bone, result in the activation of canonical Wnt signaling, increasing osteoblast differentiation and bone formation, and thereby bone mass: 1/ Global haplo-insufficient or *Runx2-Cre* driven depletion of *Rspo3* increased bone mass, OB numbers, and BFR in mice long bones; 2/ Ex vivo, haplo-insufficient BMSCs exhibited increased OB differentiation and canonical Wnt signaling; 3/ *Rspo3* null MEFs also exhibited an enhanced Wnt signaling activity; 4/ Basal levels of Erk phosphorylation were high in these cells and inhibition of Erk phosphorylation prevented the activation of Wnt signaling; 5/ *Rspo3* haplo-insufficiency rescued partially the inhibition of Wnt signaling induced by *Dkk1* *in vitro* and *in vivo*.

In vitro studies have demonstrated that overexpression of and treatment with *Rspo1* or *Rspo2* enhance Wnt ligand-mediated OB differentiation^{9, 10, 28}. The literature and our own *in vitro* studies

confirm that *Rspo3* can be, as expected, a co-activator of canonical Wnt signaling in the Topflash assay, potentiating Wnt3a-dependent activation of canonical Wnt signaling in cellular assays (⁵⁷ and Figure 6- figure supplement 1). However, the expression of canonical Wnt target genes and the levels of pLrp6, activated β -catenin and Tcf1 were also markedly increased in *Rspo3* haplo-insufficient BMSCs and in *Rspo3*-null MEFs, independent of the addition of Wnt3a to the assays, indicating that, counter-intuitively, the decrease or absence of *Rspo3* activates mechanisms that favor β -catenin-dependent signaling. This is in contrast with the data reported by Nilsson *et al.* who show a decrease in Dkk1 and Sost, but this was done in the vertebrae of *Runx2-CreRspo3^{fl/fl}* mice, where BFR is in fact decreased, or a decrease in *Tcf7* and *Lef1* expression in calvarial OBs (cortical-derived cells ⁵⁸) treated with and without Tamoxifen to induce *Rspo3* deletion *in vitro* ⁴⁰, when cortical bone is in fact not affected. Although we have not analyzed mRNA expression in the vertebrae or calvaria, our extensive set of data (Topflash, Q-RTPCR, Western blot analysis for several Wnt signaling downstream proteins) using different cells (BMSC and MEFs) and long bones clearly show an activation of Wnt signaling with *Rspo3* haploinsufficiency or deletion.

Another new finding from our studies is that *Rspo3* expression is strongly repressed by Wnt3a and increased by Dkk1. This, together with the results discussed above, suggests that *Rspo3* may provide a negative feedback-loop helping to balance canonical Wnt activity. Dkk1 efficacy in blocking Wnt3a-dependent activation of canonical Wnt signaling is significantly impaired in the absence of *Rspo3* and *Rspo3* haplo-insufficiency antagonizes the inhibition of bone formation induced by OB-targeted expression of Dkk1, confirming *in vivo* that *Rspo3* haplo-insufficiency counteracts the OB-Dkk1 dependent function. Our results show that this is the result of intracellular changes in alternative pathways regulated by *Rspo3*. Indeed, we found that the Erk signaling pathway is activated and the basal level of Lrp6 phosphorylation enhanced by *Rspo3* depletion. Thus, the activation of the Wnt signaling pathway when *Rspo3* is expressed at low levels results from intra-cellular changes, distal to the receptor complexes. Our data and that of others ²³ suggest that there are alternate *Rspo3*-

mediated signaling mechanisms, separate from the Fzd/Lrp/ β -catenin Wnt pathway, including the Wnt/PCP signaling^{14, 15} and that these events can in turn regulate Wnt signaling intra-cellularly, such that β -catenin can be stabilized independent of the proximal activation of the canonical Wnt signaling machinery through changes in other signaling pathways^{3, 53, 58}.

Thus, deletion of *Rspo3* enhances Erk signaling which, in turn, stabilizes β -catenin independent of the canonical Wnt signaling receptor complex. In turn, this has a positive effect on OB differentiation^{50, 52, 53}. Our finding that the increase in Wnt signaling activation and the OB potential of MSCs seen in the absence of *Rspo3* is abrogated by blocking Erk signaling confirms that the activation of Erk signaling associated with *Rspo3* deficiency is responsible, at least in part, for the observed Wnt signaling activation.

Supporting our findings, *in vitro* studies have shown that *Rspo3* silencing activates Erk signaling downstream of Lgr4, leading to increased OB differentiation of human adipose-derived stem cells⁴². This study did not however establish a connection between Erk and Wnt signaling. Although Lgrs function as receptors for Rspos, and Rspos/Lgrs interactions enhance Wnt signaling by inducing the clearance of Rnf43 and Znf3^{16, 17, 59}, there is also strong evidence that Rspos/Lgrs interaction can activate distinct signaling cascades that can affect bone, including the cAMP/PKA/Creb signaling pathway in Lgr4 null mice⁶⁰ and the Erk signaling cascade^{42, 61-63}.

Based on our observations, we propose that *Rspo3* has a dual mode of action to regulate canonical Wnt signaling and bone formation. This duality is based on the regulation of two distinct signaling cascades and their crosstalk: *Rspo3* functions via both the Lgr/Rnf43/Znf3 and the Lgr/Erk axes, and while activation of the Lgr/Rnf43/Znf3 axis boosts Wnt signaling strength by the membrane clearance of Rnf43/Znf3 and subsequent stabilization of Fzd receptors, binding of *Rspo3* to Lgr impairs Erk signaling, preventing Erk signaling activation and further stabilization of β -catenin (Figure 10). Thus, haplo-insufficiency and deletion of *Rspo3* would dampen Wnt signaling at the cell surface by preventing the Rnf43/Znf3 effects while intracellularly enhancing pLrp6 and β -catenin

356 stabilization, via Erk phosphorylation, overcompensating the decrease in Rspo3-dependent Lrp5/6
357 receptors-dependent Wnt activation in OBs and their progenitors. Because activation of the
358 Lgr/Rnf43/Znrf3 cascade is not exclusively dependent on Rspo3, deletion of *Rspo3* would only hinder
359 canonical Wnt signaling partially. In contrast, lack of *Rspo3* promotes the Lgr/Erk cascade, to not only
360 enhance β -catenin stabilization (Figure 10) but also regulate OB differentiation and bone formation.
361 This model also explains the observed loss of Dkk1 efficacy in inhibiting Wnt signaling: the Erk-
362 dependent stabilization of β -catenin being independent of Wnt receptor activation, Dkk1, which binds
363 to the LRP5/6 receptors, cannot dampen the activation of downstream events as they are
364 independent of the LRP5/6-Fzd receptor complex.

365 Supporting the fact that Rspo3 can also regulate Wnt-independent pathways, a recent study has
366 suggested that Rspo3 acts as an antagonist to BMPR1A, inhibiting BMP signaling during
367 development²³. Thus, our observations may be due, at least in part, to changes (activation) in BMP
368 signaling, which in turn could lead to the observed increase in pErk⁴⁹. Although this remains a
369 possibility, it seems unlikely. First, in contrast to our observations here, BMP activation in the adult
370 skeleton has been linked to activation of non-canonical Wnt signaling, increased Sost expression and
371 bone resorption^{56, 64}. Second, several studies have shown that activation of BMP signaling in the
372 osteoblast lineage has a negative impact on bone formation and bone mass⁶⁵⁻⁶⁸.

373 In conclusion, our studies indicate that Rspo3 is required for skeletal homeostasis and show for the
374 first time that axial and appendicular skeleton are differentially regulated by this Wnt signaling
375 regulator. The molecular basis for this differential regulation has not been elucidated but might
376 include different embryologic origin, differences in local micro-environment or differences in
377 mechanical loading, for instance. Nevertheless, our *in vitro* studies suggest that Rspo3 regulates
378 bone formation through its interaction not only with the Wnt receptor machinery, as a positive co-
379 activator, but also with other signaling pathways that affect β -catenin stability independent of the
380 receptor complexes. Consequently, its deletion removes a co-activator of Wnt signaling, potentially

decreasing bone formation, but also promotes Erk signaling activation, increasing β -catenin stability sufficiently to enhance bone formation and increase bone mass in the appendicular skeleton. Furthermore, because *Rspo3* depletion increases *Dkk1* and *Dkk1* increases *Rspo3* expression, this study also reveals a novel *Rspo3*-dependent negative feedback Wnt signaling regulatory loop. These findings have important implications for understanding the pleiotropic functions of *Rsp* and Wnt signaling in skeletal homeostasis and the mechanisms that regulate bone mass.

Materials and methods

Biological variables and reproducibility

To conduct the proposed studies, we insured strict application of scientific methods that supports robust and unbiased design, analysis, interpretation, and reporting of results, and sufficient information for all studies undertaken. *In vivo* analysis was performed in males and females, at different ages, and in the axial and appendicular skeleton. *Rspo3*^{+/-} mice and *Rspo3*-OB-cKO mice with targeted deletion of *Rspo3* in osteoprogenitors (*Runx2-Cre*) were investigated. Given that our studies with *Rspo3* mutant mice do not identify sex differences, and the osteoblast specific *Dkk1* transgenic (*Dkk1-Tg*) mice did not show sex differences⁴⁸, studies including crossing with the two strains were performed in female mice. To avoid bias, data were collected in a blinded fashion, in that the observer was unaware of the experimental groups and more than one individual performed key studies. *In vivo* studies were performed with *n*=4-10 mice per genotype. We based this number on a *priori* calculations for power to detect differences in the primary outcome skeletal phenotype by histomorphometric analysis. We found that based on three independent methods for measuring the skeletal phenotype 4-10 mice per group provide enough power (80% to 90%) to find statistical significance at *p*< 0.05. *Ex vivo* and *in vitro* studies involved at least three biological replicates per group/treatment.

Animals

Rspo3^{+/-} and *Rspo3*^{fl} mice were provided by Dr. Christof Niehrs (DKFZ-ZMBH Alliance, Germany) and were previously described ²⁷. The osteoblast specific *Dkk1* transgenic (*Dkk1-Tg*) mice, expressing high levels of *Dkk1* in osteoblasts, were generously provided by Dr. Guo and Dr. Kronenberg (Massachusetts General Hospital, MA, USA) ⁴⁸. *Runx2-Cre* mice were provided by Dr. Tuckermann (Ulm University, Ulm, Germany) ⁴⁵. All experiments were performed with age- and sex-matched littermates. All animals are in the C57BL/6 background and were housed in the Harvard Center for Comparative Medicine and all experimental procedures were approved by the Harvard University Institutional Animal Care and Use Committee. The protocol number associated with the ethical approval of the animal work is IS1045.

Skeletal phenotype

For bone histomorphometric analysis of *Rspo3*^{+/-} mice, 6, 12 or 18 week (wk)-old mice were injected with 20 mg/kg of calcein and 40 mg/kg of demeclocycline (Sigma Aldrich, St. Louis, MO, USA) 6, 8 or 9 days, respectively and 2 days prior to the sacrifice. For mice with *Rspo3* deletion in *Runx2*⁺ cells, 8-wk-old mice were injected with 20 mg/kg of calcein and 40 mg/kg of demeclocycline, 8 and 2 days prior to sacrifice and for the experiments with the *Dkk1-Tg* mice, 6-wk-old mice were injected 6 and 2 days prior to sacrifice. Bone histomorphometric analysis was performed within the proximal tibia under 200X magnification in a 0.9-mm high and 1.3-mm-wide region where was 200 µm away from the growth plate. For vertebra analysis, data were obtained under 200X magnification in a 1.3mm x 1.8mm region away from the growth plate to avoid including primary spongiosa. Consecutive sections of the proximal tibia and frontal sections of the vertebral body (4 µm thickness) were stained with von Kossa and Toluidine blue for the analysis of cellular parameters and osteoid. Bone sections were viewed with a Nikon E800 microscope equipped with Olympus DP71 digital camera (RRID:SCR_020326). Images were captured using Olympus CellSens software (RRID:SCR_014551). The OsteoMeasure analyzing software (Osteometrics) was used to generate and calculate the data. Structural parameters (bone volume fraction (BV/TV), trabecular thickness

(Tb.Th), trabecular number (Tb.N), and trabecular separation (Tb.Sp) were obtained by calculating the average of 2 different measurements from consecutive sections. The structural, dynamic, and cellular parameters were presented according to the standardized nomenclature⁶⁹.

A high-resolution desktop micro-tomographic imaging system (μ CT40, Scanco Medical AG, RRID:SCR_017119, Brüttisellen, Switzerland) was used to assess trabecular bone architecture and mineral density in the L5 vertebral body and femur and cortical bone architecture in the diaphysis of the femur or the tibia. Scans were acquired using a $10\text{ }\mu\text{m}^3$ isotropic voxel size, 70 kVP, 114 mAs, and 200 ms integration time. μ CT scanning and analysis were performed according to recommended guidelines (). Trabecular bone within this region was segmented from soft tissue using a threshold of 400 mg HA/cm^3 . The Scanco trabecular morphology evaluation script was used to measure trabecular bone volume fraction (Tb.BV/TV, %), trabecular bone mineral density (Tb.BMD, mg HA/cm³), Tb.N (mm⁻¹), Tb.Th (μ m), Tb.Sp (μ m), structural model index (SMI), and connectivity density (Conn.D, mm⁻³). Cortical bone was assessed in 500 μ m long regions (50 transverse slices) at the femoral mid-diaphysis and tibial diaphysis (2mm superior to the distal tibiofibular junction). Images within the cortical region of interest were segmented using a threshold of 700 mgHA/cm^3 and then the Scanco midshaft evaluation script was used to measure total cross-sectional area Total area (Tt.Ar, mm²), cortical bone area (Ct.Ar, mm²), medullary area (Ma.Ar, mm²), bone area fraction (Ct.Ar/Tt.Ar, %), cortical tissue mineral density (Ct.TMD, mgHA/cm³), cortical thickness (Ct.Th, mm).

Flow cytometry

Bone marrow was analyzed by flow cytometry as previously described⁴⁴. Briefly, bone marrow cells were flushed from femurs and tibiae of 6-8-wk old WT or *Rspo3*^{+/-} mice and washed with Hank's Balanced Salt Solution (HBSS). Residual bone samples were further digested in 3 mg/ml type I collagenase (Worthington Biochemical Corp., Lakewood, NJ 08701, USA) for 1 hour at 37°C and released cells were mixed with flushed bone marrow cells. Cells were stained with LIVE/DEAD® Fixable Aqua Dead Cell Stain Kit (Thermo Fisher Scientific, Waltham, MA, USA), AF700-anti-lineage

(RRID:AB_2715571), PE-anti-CD31 (RRID:AB_2572182), PB-anti-Sca-1 (RRID:AB_2143237), anti-Cy7APC-CD45 (RRID:AB_2860726), and biotin-anti-CD51 (RRID:AB_313073) with streptavidin-APC antibodies (BioLegend, San Diego, CA, USA). Cells were analyzed on a BD FACS ARIAll (RRID:SCR_018091) upon exclusion of dead cells.

Bone marrow stromal cells and calvarial osteoblasts

Bone marrow cells were flushed from femurs and tibiae of 6-8 wk-old WT or *Rspo3*^{+/-} mice and cultured in DMEM supplemented with 10% fetal bovine serum (FBS) and 1% penicillin (100 U/ml) and streptomycin (100 µg/ml) for 3 days (GIBCO, Thermo Fisher Scientific, Waltham, MA, USA). Adherent MSCs were counted, re-plated onto at a 5,000/cm² density and RNA or protein isolated 3 days later. For colony forming unit assays, flushed bone marrow stromal cells were plated (3X10⁶/6 wells) for CFU- (Fibroblast) F and CFU-OB assays. Cells were treated either with recombinant mouse *Rspo3* (100 ng/ml) (all from R&D system, Minneapolis, MN, USA) or U0126 (10µM) (Selleckchem, Houston TX, USA). CFU-F was detected by staining with 0.2% crystal violet in 2% ethanol for 1 hour after 10 days in culture and CFU-OB was detected by alkaline phosphatase activity with Naphthol AS-MX, n,n-dimethylformamide and Fast Blue RR salt (Sigma Aldrich, St. Louis, MO, USA) after 12 days in culture with OB differentiation medium: DMEM supplemented with 10%FBS, 1% penicillin (100 U/ml) and streptomycin (100 µg/ml) (GIBCO, Thermo Fisher Scientific, Waltham, MA, USA), 5µg/ml ascorbic acid and 10 mM β-glycerolphospahte (Sigma-Aldrich, St. Louis, MO, USA). Calvarial OBs were isolated from 1-3-day old pups via serial enzymatic digestions and cultured as previously reported ⁷⁰.

Mouse Embryonic Fibroblasts (MEFs) primary culture

To obtain WT and *Rspo3*^{-/-} MEFs, *Rspo3*^{+/-} males and females were crossed, and the morning of vaginal plug detection was defined as embryonic day (E) 0.5. At E9.5, whole embryos were isolated, washed in PBS, minced in 0.05% trypsin (GIBCO, Thermo Fisher Scientific, Waltham, MA, USA) followed by incubation at 37C for 10 min. After incubation samples were pipetted to obtain single cell

suspension and cells cultured in DMEM supplemented with 10% FBS and 1% penicillin/streptomycin. All the experiments were performed in passage 4 to 6 of WT or *Rspo3*^{-/-} MEFs. Cells were treated either 50 or 200 ng/ml of recombinant human Wnt3a, recombinant human Dkk1 (50-400 ng/ml), recombinant human and/or mouse Rspo3 (100 ng/ml) (all from R&D system, Minneapolis, MN, USA) or U0126 (10μM) (Selleckchem, Houston TX, USA). For TOPflash luciferase reporter assay, cells were transiently co-transfected with 400 ng TOPflash-luc reporter plasmid (RRID:Addgene_12456) and 10 ng control pCMV-Renilla-luciferase (RRID:Addgene_45968, Promega, Madison WI, USA) using Lipofectamine 2000 (Invitrogen, Thermo Fisher Scientific, Waltham, MA, USA) according to the manufacturers protocol. Cells were subjected to serum starvation in DMEM containing 1% FBS overnight. Cells were subsequently treated with recombinant human Wnt3a in the presence and absence of increasing concentration of Dkk1 for 24 hours followed by luciferase assay using the Dual-Glo Assay system (Promega, Madison WI, USA) according to the manufacturers protocol. Data were normalized by Renilla-firefly activity and presented as fold change compared to control group.

Osteoclast Primary Culture and mix-matched co-cultures

Murine bone marrow macrophages were isolated from bone marrow flushed tibiae and femurs of WT and *Rspo3*^{+/-} mice at 6 to 8-wk-old as described previously⁷⁰. Briefly, cells were cultured in complete α-MEM with 30 ng/ml macrophage colony-stimulating factor M-CSF (R&D system, Minneapolis, MN, USA) in suspension culture dish to which stromal cells and lymphoid cells cannot adhere, at 37 °C for 2-3 days. For osteoclast generation, cells were cultured in 30 ng/ml M-CSF and 10 ng/ml RANKL (R&D systems, Minneapolis, MN, USA). For co-culture experiments, mouse calvarial osteoblasts were isolated from newborn WT and *Rspo3*^{+/-} as previously reported^{46, 70} and seeded in 96-well plates (2,000 cells/well) in complete osteogenic α-MEM containing 100 nM Vitamin D3 and 1 μM prostaglandin E2 (Enzo Life Science, Farmingdale, NY, USA). After 3 days, 10,000 BMM from WT and *Rspo3*^{+/-} mice at 6 to 8-week-old mice were added per well and cocultured for 9 days in complete osteogenic α-MEM. Tartrate-resistant acid phosphatase (TRAP) staining was

performed to evaluate the number of osteoclasts according to the manufacture's protocol (Sigma-Aldrich, St. Louis, MO, USA).

Western Blot analysis

Five μ g of total proteins were resolved by SDS-PAGE under reducing conditions. Immunodetection was performed with antibodies specific to: Active β -catenin, phosphorylated (p) Lrp6, p-Erk, total Erk, Tcf1, Lrp6 and Tubulin [(CST8814, RRID:AB_11127203) (CST2568, RRID:AB_2139327) (CST9101, RRID:AB_331646), (CST9102, RRID:AB_330744), (CST2203, RRID:AB_2199302), (CST3395, RRID:AB_1950408), (CST2125, RRID:AB_2619646) Cell Signaling, Beverly, MA, USA] GAPDH and Actin [(SC32233, RRID:AB_627678) and (SC47778, RRID:AB_626632) Santa Cruz, Santa Cruz, CA, USA]. Immunoreactivities were assessed using ECL plus kit following the manufacture's protocol (Perkin Elmer, Waltham, MA, USA). Quantification was performed using Image J (RRID:SCR_003070)

Protein levels were normalized to the levels of housekeeping protein or total protein in within the same sample.

Quantitative-Real Time PCR

Total RNA was isolated from cells using the RNeasy Mini Kit (Qiagen Germantown, MD, USA) according to the manufacturer's protocols. Total RNA from cortical bone of WT and *Rspo3*^{+/-} mice was extracted using Trizol reagent (Invitrogen) followed by RNeasy Micro Kit (Qiagen Germantown, MD, USA) according to the manufacturer's protocols. cDNA was synthesized using iScript cDNA synthesis kit (BIO-RAD. Hercules, CA, USA) and quantitative real time PCR performed. mRNA levels encoding each gene of interest were normalized for β 2M or actin mRNA in the same sample and the relative expression of the genes of interest was determined using the formula of Livak and Schmittgen⁷¹. Data are presented as fold change relative to WT cells or animals.

Statistical analysis

Data are expressed as the mean \pm SEM. All experiments include at least three biological replicates and were done in duplicate or triplicate. Values represent the number of biological replicates. Statistical analysis was conducted using unpaired two-tail Student's t-test, or Two-Way ANOVA followed by post-hoc test for multiple comparisons. GraphPad PRISM 9 (RRID:SCR_002798) was also used for statistical analysis. A two-sided p-value of <0.05 was considered as the threshold for statistical significance.

Reference

1. Clevers H, Nusse R. Wnt/beta-catenin signaling and disease. *Cell*. 2012;149(6):1192-205. Epub 2012/06/12. doi: 10.1016/j.cell.2012.05.012. PubMed PMID: 22682243.
2. Nusse R, Clevers H. Wnt/beta-Catenin Signaling, Disease, and Emerging Therapeutic Modalities. *Cell*. 2017;169(6):985-99. Epub 2017/06/03. doi: 10.1016/j.cell.2017.05.016. PubMed PMID: 28575679.
3. Baron R, Kneissel M. WNT signaling in bone homeostasis and disease: from human mutations to treatments. *Nat Med*. 2013;19(2):179-92. doi: 10.1038/nm.3074. PubMed PMID: 23389618.
4. Gori F, Baron, R. Wnt signaling in skeletal homeostasis and diseases. *Osteoporosis, Fifth Edition Academic Press Elsevier*. 2021:257-79.
5. Huybrechts Y, Mortier G, Boudin E, Van Hul W. WNT Signaling and Bone: Lessons From Skeletal Dysplasias and Disorders. *Front Endocrinol (Lausanne)*. 2020;11:165. Epub 2020/04/25. doi: 10.3389/fendo.2020.00165. PubMed PMID: 32328030; PMCID: PMC7160326.
6. Baron R, Gori F, Leder BZ. Sclerostin Inhibition in the Treatment of Osteoporosis. *Osteoporosis Pathophysiology and Clinical Management Editors: Leder BZ and Wein MN Springer Third Edition*. 2020:375.
7. de Lau W, Peng WC, Gros P, Clevers H. The R-spondin/Lgr5/Rnf43 module: regulator of Wnt signal strength. *Genes Dev*. 2014;28(4):305-16. Epub 2014/02/18. doi: 10.1101/gad.235473.113. PubMed PMID: 24532711; PMCID: PMC3937510.

8. de Lau WB, Snel B, Clevers HC. The R-spondin protein family. *Genome Biol.* 2012;13(3):242. Epub 2012/03/24. doi: 10.1186/gb-2012-13-3-242. PubMed PMID: 22439850; PMCID: PMC3439965.
9. Knight MN, Hankenson KD. R-spondins: novel matricellular regulators of the skeleton. *Matrix Biol.* 2014;37:157-61. Epub 2014/07/02. doi: 10.1016/j.matbio.2014.06.003. PubMed PMID: 24980904.
10. Lu W, Kim KA, Liu J, Abo A, Feng X, Cao X, Li Y. R-spondin1 synergizes with Wnt3A in inducing osteoblast differentiation and osteoprotegerin expression. *FEBS Lett.* 2008;582(5):643-50. Epub 2008/02/05. doi: 10.1016/j.febslet.2008.01.035. PubMed PMID: 18242177.
11. Nagano K. R-spondin signaling as a pivotal regulator of tissue development and homeostasis. *Jpn Dent Sci Rev.* 2019;55(1):80-7. Epub 2019/05/03. doi: 10.1016/j.jdsr.2019.03.001. PubMed PMID: 31049116; PMCID: PMC6479641.
12. Raslan AA, Yoon JK. R-spondins: Multi-mode WNT signaling regulators in adult stem cells. *Int J Biochem Cell Biol.* 2019;106:26-34. Epub 2018/11/16. doi: 10.1016/j.biocel.2018.11.005. PubMed PMID: 30439551.
13. Shi GX, Mao WW, Zheng XF, Jiang LS. The role of R-spondins and their receptors in bone metabolism. *Prog Biophys Mol Biol.* 2016;122(2):93-100. Epub 2016/05/31. doi: 10.1016/j.pbiomolbio.2016.05.012. PubMed PMID: 27237581.
14. Glinka A, Dolde C, Kirsch N, Huang YL, Kazanskaya O, Ingelfinger D, Boutros M, Cruciat CM, Niehrs C. LGR4 and LGR5 are R-spondin receptors mediating Wnt/beta-catenin and Wnt/PCP signalling. *EMBO Rep.* 2011;12(10):1055-61. Epub 2011/09/13. doi: 10.1038/embor.2011.175. PubMed PMID: 21909076; PMCID: PMC3185347.
15. Hao HX, Xie Y, Zhang Y, Charlat O, Oster E, Avello M, Lei H, Mickanin C, Liu D, Ruffner H, Mao X, Ma Q, Zamponi R, Bouwmeester T, Finan PM, Kirschner MW, Porter JA, Serluca FC, Cong F. ZNRF3 promotes Wnt receptor turnover in an R-spondin-sensitive manner. *Nature.* 2012;485(7397):195-200. Epub 2012/05/12. doi: 10.1038/nature11019. PubMed PMID: 22575959.

16. Ruffner H, Sprunger J, Charlat O, Leighton-Davies J, Grosshans B, Salathe A, Zietzling S, Beck V, Therier M, Isken A, Xie Y, Zhang Y, Hao H, Shi X, Liu D, Song Q, Clay I, Hintzen G, Tchorz J, Bouchez LC, Michaud G, Finan P, Myer VE, Bouwmeester T, Porter J, Hild M, Bassilana F, Parker CN, Cong F. R-Spondin potentiates Wnt/beta-catenin signaling through orphan receptors LGR4 and LGR5. *PLoS One*. 2012;7(7):e40976. Epub 2012/07/21. doi: 10.1371/journal.pone.0040976. PubMed PMID: 22815884; PMCID: PMC3397969.
17. Wang D, Huang B, Zhang S, Yu X, Wu W, Wang X. Structural basis for R-spondin recognition by LGR4/5/6 receptors. *Genes Dev*. 2013;27(12):1339-44. Epub 2013/06/13. doi: 10.1101/gad.219360.113. PubMed PMID: 23756652; PMCID: PMC3701189.
18. Xie Y, Zamponi R, Charlat O, Ramones M, Swalley S, Jiang X, Rivera D, Tschantz W, Lu B, Quinn L, Dimitri C, Parker J, Jeffery D, Wilcox SK, Watrobka M, LeMotte P, Granda B, Porter JA, Myer VE, Loew A, Cong F. Interaction with both ZNRF3 and LGR4 is required for the signalling activity of R-spondin. *EMBO Rep*. 2013;14(12):1120-6. Epub 2013/10/30. doi: 10.1038/embor.2013.167. PubMed PMID: 24165923; PMCID: PMC3981092.
19. Lebensohn AM, Rohatgi R. R-spondins can potentiate WNT signaling without LGRs. *Elife*. 2018;7. Epub 2018/02/07. doi: 10.7554/eLife.33126. PubMed PMID: 29405118; PMCID: PMC5800842.
20. Szenker-Ravi E, Altunoglu U, Leushacke M, Bosso-Lefevre C, Khatoor M, Thi Tran H, Naert T, Noelanders R, Hajamohideen A, Beneteau C, de Sousa SB, Karaman B, Latypova X, Basaran S, Yucel EB, Tan TT, Vlamincx L, Nayak SS, Shukla A, Girisha KM, Le Caignec C, Soshnikova N, Uyguner ZO, Vlamincx K, Barker N, Kayserili H, Reversade B. RSPO2 inhibition of RNF43 and ZNRF3 governs limb development independently of LGR4/5/6. *Nature*. 2018;557(7706):564-9. Epub 2018/05/18. doi: 10.1038/s41586-018-0118-y. PubMed PMID: 29769720.
21. Rong X, Chen C, Zhou P, Zhou Y, Li Y, Lu L, Liu Y, Zhou J, Duan C. R-spondin 3 regulates dorsoventral and anteroposterior patterning by antagonizing Wnt/beta-catenin signaling in zebrafish

embryos. PLoS One. 2014;9(6):e99514. Epub 2014/06/12. doi: 10.1371/journal.pone.0099514. PubMed PMID: 24918770; PMCID: PMC4053527.

22. Wu C, Qiu S, Lu L, Zou J, Li WF, Wang O, Zhao H, Wang H, Tang J, Chen L, Xu T, Sun Z, Liao W, Luo G, Lu X. RSPO2-LGR5 signaling has tumour-suppressive activity in colorectal cancer. Nat Commun. 2014;5:3149. Epub 2014/01/31. doi: 10.1038/ncomms4149. PubMed PMID: 24476626.

23. Lee H, Seidl C, Sun R, Glinka A, Niehrs C. R-spondins are BMP receptor antagonists in *Xenopus* early embryonic development. Nat Commun. 2020;11(1):5570. Epub 2020/11/06. doi: 10.1038/s41467-020-19373-w. PubMed PMID: 33149137; PMCID: PMC7642414.

24. Aoki M, Mieda M, Ikeda T, Hamada Y, Nakamura H, Okamoto H. R-spondin3 is required for mouse placental development. Dev Biol. 2007;301(1):218-26. Epub 2006/09/12. doi: 10.1016/j.ydbio.2006.08.018. PubMed PMID: 16963017.

25. Neufeld S, Rosin JM, Ambasta A, Hui K, Shaneman V, Crowder R, Vickerman L, Cobb J. A conditional allele of *Rspo3* reveals redundant function of R-spondins during mouse limb development. Genesis. 2012;50(10):741-9. Epub 2012/05/23. doi: 10.1002/dvg.22040. PubMed PMID: 22610508.

26. Ishii Y, Wajid M, Bazzi H, Fantauzzo KA, Barber AG, Blaydon DC, Nam JS, Yoon JK, Kelsell DP, Christiano AM. Mutations in R-spondin 4 (RSPO4) underlie inherited anonychia. J Invest Dermatol. 2008;128(4):867-70. Epub 2007/09/07. doi: 10.1038/sj.jid.5701078. PubMed PMID: 17805348.

27. Kazanskaya O, Ohkawara B, Herault M, Wu W, Maltry N, Augustin HG, Niehrs C. The Wnt signaling regulator R-spondin 3 promotes angioblast and vascular development. Development. 2008;135(22):3655-64. Epub 2008/10/10. doi: 10.1242/dev.027284. PubMed PMID: 18842812.

28. Knight MN, Karuppaiah K, Lowe M, Mohanty S, Zondervan RL, Bell S, Ahn J, Hankenson KD. R-spondin-2 is a Wnt agonist that regulates osteoblast activity and bone mass. Bone Res. 2018;6:24. Epub 2018/08/23. doi: 10.1038/s41413-018-0026-7. PubMed PMID: 30131881; PMCID: PMC6089978 Skelegen. The remaining authors declare no competing interests.

29. Park S, Cui J, Yu W, Wu L, Carmon KS, Liu QJ. Differential activities and mechanisms of the four R-spondins in potentiating Wnt/beta-catenin signaling. *J Biol Chem*. 2018;293(25):9759-69. Epub 2018/05/13. doi: 10.1074/jbc.RA118.002743. PubMed PMID: 29752411; PMCID: PMC6016459.
30. Parma P, Radi O, Vidal V, Chaboissier MC, Dellambra E, Valentini S, Guerra L, Schedl A, Camerino G. R-spondin1 is essential in sex determination, skin differentiation and malignancy. *Nat Genet*. 2006;38(11):1304-9. Epub 2006/10/17. doi: 10.1038/ng1907. PubMed PMID: 17041600.
31. Wei Q, Yokota C, Semenov MV, Doble B, Woodgett J, He X. R-spondin1 is a high affinity ligand for LRP6 and induces LRP6 phosphorylation and beta-catenin signaling. *J Biol Chem*. 2007;282(21):15903-11. Epub 2007/04/03. doi: 10.1074/jbc.M701927200. PubMed PMID: 17400545.
32. Nam JS, Turcotte TJ, Yoon JK. Dynamic expression of R-spondin family genes in mouse development. *Gene Expr Patterns*. 2007;7(3):306-12. Epub 2006/10/13. doi: 10.1016/j.modgep.2006.08.006. PubMed PMID: 17035101.
33. Alhazmi N, Carroll SH, Kawasaki K, Woronowicz KC, Hallett SA, Macias Trevino C, Li EB, Baron R, Gori F, Yelick PC, Harris MP, Liao EC. Synergistic roles of Wnt modulators R-spondin2 and R-spondin3 in craniofacial morphogenesis and dental development. *Sci Rep*. 2021;11(1):5871. Epub 2021/03/14. doi: 10.1038/s41598-021-85415-y. PubMed PMID: 33712657; PMCID: PMC7954795.
34. Duncan EL, Danoy P, Kemp JP, Leo PJ, McCloskey E, Nicholson GC, Eastell R, Prince RL, Eisman JA, Jones G, Sambrook PN, Reid IR, Dennison EM, Wark J, Richards JB, Uitterlinden AG, Spector TD, Esapa C, Cox RD, Brown SD, Thakker RV, Addison KA, Bradbury LA, Center JR, Cooper C, Cremin C, Estrada K, Felsenberg D, Gluer CC, Hadler J, Henry MJ, Hofman A, Kotowicz MA, Makovey J, Nguyen SC, Nguyen TV, Pasco JA, Pryce K, Reid DM, Rivadeneira F, Roux C, Stefansson K, Styrkarsdottir U, Thorleifsson G, Tichawangana R, Evans DM, Brown MA. Genome-wide association study using extreme truncate selection identifies novel genes affecting bone mineral density and fracture risk. *PLoS Genet*. 2011;7(4):e1001372. Epub 2011/05/03. doi: 10.1371/journal.pgen.1001372. PubMed PMID: 21533022; PMCID: PMC3080863.

653 35. Estrada K, Styrkarsdottir U, Evangelou E, Hsu YH, Duncan EL, Ntzani EE, Oei L, Albagha OM,
 654 Amin N, Kemp JP, Koller DL, Li G, Liu CT, Minster RL, Moayyeri A, Vandenput L, Willner D, Xiao SM,
 655 Yerges-Armstrong LM, Zheng HF, Alonso N, Eriksson J, Kammerer CM, Kaptoge SK, Leo PJ,
 656 Thorleifsson G, Wilson SG, Wilson JF, Aalto V, Alen M, Aragaki AK, Aspelund T, Center JR, Dailiana
 657 Z, Duggan DJ, Garcia M, Garcia-Giralt N, Giroux S, Hallmans G, Hocking LJ, Husted LB, Jameson
 658 KA, Khusainova R, Kim GS, Kooperberg C, Koromila T, Kruk M, Laaksonen M, Lacroix AZ, Lee SH,
 659 Leung PC, Lewis JR, Masi L, Mencej-Bedrac S, Nguyen TV, Nogues X, Patel MS, Prezelj J, Rose
 660 LM, Scollen S, Siggeirsdottir K, Smith AV, Svensson O, Trompet S, Trummer O, van Schoor NM,
 661 Woo J, Zhu K, Balcells S, Brandi ML, Buckley BM, Cheng S, Christiansen C, Cooper C, Dedoussis G,
 662 Ford I, Frost M, Goltzman D, Gonzalez-Macias J, Kahonen M, Karlsson M, Khusnutdinova E, Koh
 663 JM, Kollia P, Langdahl BL, Leslie WD, Lips P, Ljunggren O, Lorenc RS, Marc J, Mellstrom D,
 664 Obermayer-Pietsch B, Olmos JM, Pettersson-Kymmer U, Reid DM, Riancho JA, Ridker PM,
 665 Rousseau F, Slagboom PE, Tang NL, Urreizti R, Van Hul W, Viikari J, Zarrabeitia MT, Aulchenko YS,
 666 Castano-Betancourt M, Grundberg E, Herrera L, Ingvarsson T, Johannsdottir H, Kwan T, Li R, Luben
 667 R, Medina-Gomez C, Palsson ST, Reppe S, Rotter JI, Sigurdsson G, van Meurs JB, Verlaan D,
 668 Williams FM, Wood AR, Zhou Y, Gautvik KM, Pastinen T, Raychaudhuri S, Cauley JA, Chasman DI,
 669 Clark GR, Cummings SR, Danoy P, Dennison EM, Eastell R, Eisman JA, Gudnason V, Hofman A,
 670 Jackson RD, Jones G, Jukema JW, Khaw KT, Lehtimäki T, Liu Y, Lorentzon M, McCloskey E,
 671 Mitchell BD, Nandakumar K, Nicholson GC, Oostra BA, Peacock M, Pols HA, Prince RL, Raitakari O,
 672 Reid IR, Robbins J, Sambrook PN, Sham PC, Shuldiner AR, Tylavsky FA, van Duijn CM, Wareham
 673 NJ, Cupples LA, Econs MJ, Evans DM, Harris TB, Kung AW, Psaty BM, Reeve J, Spector TD,
 674 Streeten EA, Zillikens MC, Thorsteinsdottir U, Ohlsson C, Karasik D, Richards JB, Brown MA,
 675 Stefansson K, Uitterlinden AG, Ralston SH, Ioannidis JP, Kiel DP, Rivadeneira F. Genome-wide
 676 meta-analysis identifies 56 bone mineral density loci and reveals 14 loci associated with risk of

fracture. *Nat Genet.* 2012;44(5):491-501. doi: 10.1038/ng.2249. PubMed PMID: 22504420; PMCID: 3338864.

36. Lee DY, Kim H, Ku SY, Kim SH, Choi YM, Kim JG. Association between polymorphisms in Wnt signaling pathway genes and bone mineral density in postmenopausal Korean women. *Menopause.* 2010;17(5):1064-70. doi: 10.1097/gme.0b013e3181da4da3. PubMed PMID: 20613673.

37. Medina-Gomez C, Kemp JP, Estrada K, Eriksson J, Liu J, Reppe S, Evans DM, Heppe DH, Vandenput L, Herrera L, Ring SM, Kruithof CJ, Timpson NJ, Zillikens MC, Olstad OK, Zheng HF, Richards JB, St Pourcain B, Hofman A, Jaddoe VW, Smith GD, Lorentzon M, Gautvik KM, Uitterlinden AG, Brommage R, Ohlsson C, Tobias JH, Rivadeneira F. Meta-analysis of genome-wide scans for total body BMD in children and adults reveals allelic heterogeneity and age-specific effects at the WNT16 locus. *PLoS Genet.* 2012;8(7):e1002718. Epub 2012/07/14. doi: 10.1371/journal.pgen.1002718. PubMed PMID: 22792070; PMCID: PMC3390371 have declared that no other competing interest exist.

38. Richards JB, Rivadeneira F, Inouye M, Pastinen TM, Soranzo N, Wilson SG, Andrew T, Falchi M, Gwilliam R, Ahmadi KR, Valdes AM, Arp P, Whittaker P, Verlaan DJ, Jhamai M, Kumanduri V, Moorhouse M, van Meurs JB, Hofman A, Pols HA, Hart D, Zhai G, Kato BS, Mullin BH, Zhang F, Deloukas P, Uitterlinden AG, Spector TD. Bone mineral density, osteoporosis, and osteoporotic fractures: a genome-wide association study. *Lancet.* 2008;371(9623):1505-12. Epub 2008/05/06. doi: 10.1016/S0140-6736(08)60599-1. PubMed PMID: 18455228; PMCID: PMC2679414.

39. Richards JB, Zheng HF, Spector TD. Genetics of osteoporosis from genome-wide association studies: advances and challenges. *Nat Rev Genet.* 2012;13(8):576-88. Epub 2012/07/19. doi: 10.1038/nrg3228. PubMed PMID: 22805710.

40. Nilsson KH, Henning P, El Shahawy M, Nethander M, Andersen TL, Ejersted C, Wu J, Gustafsson KL, Koskela A, Tuukkanen J, Souza PPC, Tuckermann J, Lorentzon M, Ruud LE, Lehtimäki T, Tobias JH, Zhou S, Lerner UH, Richards JB, Moverare-Skrtic S, Ohlsson C. RSPO3 is

important for trabecular bone and fracture risk in mice and humans. *Nat Commun.* 2021;12(1):4923. Epub 20210813. doi: 10.1038/s41467-021-25124-2. PubMed PMID: 34389713; PMCID: PMC8363747.

41. Zhu C, Zheng XF, Yang YH, Li B, Wang YR, Jiang SD, Jiang LS. LGR4 acts as a key receptor for R-spondin 2 to promote osteogenesis through Wnt signaling pathway. *Cell Signal.* 2016;28(8):989-1000. Epub 2016/05/04. doi: 10.1016/j.cellsig.2016.04.010. PubMed PMID: 27140682.

42. Zhang M, Zhang P, Liu Y, Lv L, Zhang X, Liu H, Zhou Y. RSPO3-LGR4 Regulates Osteogenic Differentiation Of Human Adipose-Derived Stem Cells Via ERK/FGF Signalling. *Sci Rep.* 2017;7:42841. Epub 2017/02/22. doi: 10.1038/srep42841. PubMed PMID: 28220828; PMCID: PMC5318871.

43. Nilsson KH, Wu J, Gustafsson KL, El Shahawy M, Koskela A, Tuukkanen J, Tuckermann J, Henning P, Lerner UH, Ohlsson C, Moverare-Skrtic S. Estradiol and RSPO3 regulate vertebral trabecular bone mass independent of each other. *Am J Physiol Endocrinol Metab.* 2022;322(3):E211-E8. Epub 20220124. doi: 10.1152/ajpendo.00383.2021. PubMed PMID: 35068191; PMCID: PMC8896994.

44. Schepers K, Pietras EM, Reynaud D, Flach J, Binnewies M, Garg T, Wagers AJ, Hsiao EC, Passegue E. Myeloproliferative neoplasia remodels the endosteal bone marrow niche into a self-reinforcing leukemic niche. *Cell Stem Cell.* 2013;13(3):285-99. Epub 2013/07/16. doi: 10.1016/j.stem.2013.06.009. PubMed PMID: 23850243; PMCID: PMC3769504.

45. Rauch A, Seitz S, Baschant U, Schilling AF, Illing A, Stride B, Kirilov M, Mandic V, Takacz A, Schmidt-Ullrich R, Ostermay S, Schinke T, Spanbroek R, Zaiss MM, Angel PE, Lerner UH, David JP, Reichardt HM, Amling M, Schutz G, Tuckermann JP. Glucocorticoids suppress bone formation by attenuating osteoblast differentiation via the monomeric glucocorticoid receptor. *Cell Metab.* 2010;11(6):517-31. Epub 2010/06/04. doi: 10.1016/j.cmet.2010.05.005. PubMed PMID: 20519123.

727 46. Moverare-Skrtic S, Henning P, Liu X, Nagano K, Saito H, Björjesson AE, Sjögren K, Windahl SH,
728 Farman H, Kindlund B, Engdahl C, Koskela A, Zhang FP, Eriksson EE, Zaman F, Hammarstedt A,
729 Isaksson H, Bally M, Kassem A, Lindholm C, Sandberg O, Aspenberg P, Savendahl L, Feng JQ,
730 Tuckermann J, Tuukkanen J, Poutanen M, Baron R, Lerner UH, Gori F, Ohlsson C. Osteoblast-
731 derived WNT16 represses osteoclastogenesis and prevents cortical bone fragility fractures. *Nat Med*.
732 2014;20(11):1279-88. Epub 2014/10/13. doi: 10.1038/nm.3654. PubMed PMID: 25306233; PMCID:
733 PMC4392888.

734 47. Li J, Sarosi I, Cattley RC, Pretorius J, Asuncion F, Grisanti M, Morony S, Adamu S, Geng Z, Qiu
735 W, Kostenuik P, Lacey DL, Simonet WS, Bolon B, Qian X, Shalhoub V, Ominsky MS, Zhu Ke H, Li X,
736 Richards WG. Dkk1-mediated inhibition of Wnt signaling in bone results in osteopenia. *Bone*.
737 2006;39(4):754-66. Epub 2006/05/30. doi: 10.1016/j.bone.2006.03.017. PubMed PMID: 16730481.

738 48. Guo J, Liu M, Yang D, Bouxsein ML, Saito H, Galvin RJ, Kuhstoss SA, Thomas CC, Schipani E,
739 Baron R, Bringham FR, Kronenberg HM. Suppression of Wnt signaling by Dkk1 attenuates PTH-
740 mediated stromal cell response and new bone formation. *Cell Metab*. 2010;11(2):161-71. Epub
741 2010/02/10. doi: 10.1016/j.cmet.2009.12.007. PubMed PMID: 20142103; PMCID: PMC2819982.

742 49. Zhou Q, Heinke J, Vargas A, Winnik S, Krauss T, Bode C, Patterson C, Moser M. ERK signaling
743 is a central regulator for BMP-4 dependent capillary sprouting. *Cardiovasc Res*. 2007;76(3):390-9.
744 Epub 2007/09/14. doi: 10.1016/j.cardiores.2007.08.003. PubMed PMID: 17850776.

745 50. Cervenka I, Wolf J, Masek J, Krejci P, Wilcox WR, Kozubik A, Schulte G, Gutkind JS, Bryja V.
746 Mitogen-activated protein kinases promote WNT/beta-catenin signaling via phosphorylation of LRP6.
747 *Mol Cell Biol*. 2011;31(1):179-89. Epub 2010/10/27. doi: 10.1128/MCB.00550-10. PubMed PMID:
748 20974802; PMCID: PMC3019858.

749 51. Gortazar AR, Martin-Millan M, Bravo B, Plotkin LI, Bellido T. Crosstalk between caveolin-
750 1/extracellular signal-regulated kinase (ERK) and beta-catenin survival pathways in osteocyte

751 mechanotransduction. J Biol Chem. 2013;288(12):8168-75. Epub 2013/01/31. doi:
752 10.1074/jbc.M112.437921. PubMed PMID: 23362257; PMCID: PMC3605635.

753 52. Kim JM, Yang YS, Park KH, Oh H, Greenblatt MB, Shim JH. The ERK MAPK Pathway Is
754 Essential for Skeletal Development and Homeostasis. Int J Mol Sci. 2019;20(8). Epub 2019/04/25.
755 doi: 10.3390/ijms20081803. PubMed PMID: 31013682; PMCID: PMC6514701.

756 53. Krejci P, Aklian A, Kaucka M, Sevcikova E, Prochazkova J, Masek JK, Mikolka P, Pospisilova T,
757 Spoustova T, Weis M, Paznekas WA, Wolf JH, Gutkind JS, Wilcox WR, Kozubik A, Jabs EW, Bryja V,
758 Salazar L, Vesela I, Balek L. Receptor tyrosine kinases activate canonical WNT/beta-catenin
759 signaling via MAP kinase/LRP6 pathway and direct beta-catenin phosphorylation. PLoS One.
760 2012;7(4):e35826. Epub 2012/05/05. doi: 10.1371/journal.pone.0035826. PubMed PMID: 22558232;
761 PMCID: PMC3338780.

762 54. Berendsen AD, Olsen BR. Bone development. Bone. 2015;80:14-8. doi:
763 10.1016/j.bone.2015.04.035. PubMed PMID: 26453494; PMCID: PMC4602167.

764 55. JUN SUN AY, Lingling Hu, Jason McCormick, Shawon Debnath, Seoyeon Bok, Yuzhe Niu, Ling
765 Zheng, Michelle Cung, Sarfaraz Lalani, Kyle Morse, Daneil Shinn, Tianna Bennett, Adrian Tan, Na Li,
766 Ren Xu, Sravisht Iyer, Matthew Greenblatt. Discovery of a vertebral stem cell driving spine metastasis
767 . Journal of Bone and Mineral Research, 2022 Annual Meeting of the American Society for Bone and
768 Mineral Research. 2022.

769 56. Simsek Kiper PO, Saito H, Gori F, Unger S, Hesse E, Yamana K, Kiviranta R, Solban N, Liu J,
770 Brommage R, Boduroglu K, Bonafe L, Campos-Xavier B, Dikoglu E, Eastell R, Gossiel F, Harshman
771 K, Nishimura G, Girisha KM, Stevenson BJ, Takita H, Rivolta C, Superti-Furga A, Baron R. Cortical-
772 Bone Fragility--Insights from sFRP4 Deficiency in Pyle's Disease. N Engl J Med. 2016;374(26):2553-
773 62. doi: 10.1056/NEJMoa1509342. PubMed PMID: 27355534; PMCID: PMC5070790.

57. Yoon JK, Lee JS. Cellular signaling and biological functions of R-spondins. *Cell Signal*. 2012;24(2):369-77. Epub 2011/10/11. doi: 10.1016/j.cellsig.2011.09.023. PubMed PMID: 21982879; PMCID: PMC3237830.

58. Azzolin L, Panciera T, Soligo S, Enzo E, Bicciato S, Dupont S, Bresolin S, Frasson C, Basso G, Guzzardo V, Fassina A, Cordenonsi M, Piccolo S. YAP/TAZ incorporation in the beta-catenin destruction complex orchestrates the Wnt response. *Cell*. 2014;158(1):157-70. Epub 2014/07/01. doi: 10.1016/j.cell.2014.06.013. PubMed PMID: 24976009.

59. de Lau W, Barker N, Low TY, Koo BK, Li VS, Teunissen H, Kujala P, Haegebarth A, Peters PJ, van de Wetering M, Stange DE, van Es JE, Guardavaccaro D, Schasfoort RB, Mohri Y, Nishimori K, Mohammed S, Heck AJ, Clevers H. Lgr5 homologues associate with Wnt receptors and mediate R-spondin signalling. *Nature*. 2011;476(7360):293-7. Epub 2011/07/06. doi: 10.1038/nature10337. PubMed PMID: 21727895.

60. Luo J, Zhou W, Zhou X, Li D, Weng J, Yi Z, Cho SG, Li C, Yi T, Wu X, Li XY, de Crombrughe B, Hook M, Liu M. Regulation of bone formation and remodeling by G-protein-coupled receptor 48. *Development*. 2009;136(16):2747-56. Epub 2009/07/17. doi: 10.1242/dev.033571. PubMed PMID: 19605502; PMCID: PMC2730404.

61. Xu P, Dang Y, Wang L, Liu X, Ren X, Gu J, Liu M, Dai X, Ye X. Lgr4 is crucial for skin carcinogenesis by regulating MEK/ERK and Wnt/beta-catenin signaling pathways. *Cancer Lett*. 2016;383(2):161-70. Epub 2016/10/25. doi: 10.1016/j.canlet.2016.09.005. PubMed PMID: 27693558.

62. Lin W, Xu L, Pan Q, Lin S, Feng L, Wang B, Chen S, Li Y, Wang H, Li Y, Wang Y, Lee WYW, Sun D, Li G. Lgr5-overexpressing mesenchymal stem cells augment fracture healing through regulation of Wnt/ERK signaling pathways and mitochondrial dynamics. *FASEB J*. 2019;33(7):8565-77. Epub 2019/04/18. doi: 10.1096/fj.201900082RR. PubMed PMID: 30991839.

63. Vieira GC, Chockalingam S, Melegh Z, Greenhough A, Malik S, Szemes M, Park JH, Kaidi A, Zhou L, Catchpoole D, Morgan R, Bates DO, Gabb PD, Malik K. LGR5 regulates pro-survival

799 MEK/ERK and proliferative Wnt/beta-catenin signalling in neuroblastoma. *Oncotarget*.
800 2015;6(37):40053-67. Epub 2015/10/31. doi: 10.18632/oncotarget.5548. PubMed PMID: 26517508;
801 PMCID: PMC4741879.

802 64. Kamiya N, Shuxian L, Yamaguchi R, Phipps M, Aruwajoye O, Adapala NS, Yuan H, Kim HK,
803 Feng JQ. Targeted disruption of BMP signaling through type IA receptor (BMPRI1A) in osteocyte
804 suppresses SOST and RANKL, leading to dramatic increase in bone mass, bone mineral density and
805 mechanical strength. *Bone*. 2016;91:53-63. doi: 10.1016/j.bone.2016.07.002. PubMed PMID:
806 27402532.

807 65. Kamiya N, Kobayashi T, Mochida Y, Yu PB, Yamauchi M, Kronenberg HM, Mishina Y. Wnt
808 inhibitors Dkk1 and Sost are downstream targets of BMP signaling through the type IA receptor
809 (BMPRI1A) in osteoblasts. *J Bone Miner Res*. 2010;25(2):200-10. doi: 10.1359/jbmr.090806. PubMed
810 PMID: 19874086; PMCID: 3153381.

811 66. Kamiya N, Ye L, Kobayashi T, Mochida Y, Yamauchi M, Kronenberg HM, Feng JQ, Mishina Y.
812 BMP signaling negatively regulates bone mass through sclerostin by inhibiting the canonical Wnt
813 pathway. *Development*. 2008;135(22):3801-11. Epub 2008/10/18. doi: 10.1242/dev.025825. PubMed
814 PMID: 18927151; PMCID: PMC2694443.

815 67. Ko FC, Van Vliet M, Ellman R, Grasso D, Brooks DJ, Spatz JM, Conlon C, Aguirre JI, Wronski
816 TJ, Bouxsein ML. Treatment With a Soluble Bone Morphogenetic Protein Type 1A Receptor
817 (BMPRI1A) Fusion Protein Increases Bone Mass and Bone Formation in Mice Subjected to Hindlimb
818 Unloading. *JBMR Plus*. 2017;1(2):66-72. Epub 2018/10/05. doi: 10.1002/jbm4.10012. PubMed PMID:
819 30283882; PMCID: PMC6124165.

820 68. Shi C, Mandair GS, Zhang H, Vanrenterghem GG, Ridella R, Takahashi A, Zhang Y, Kohn DH,
821 Morris MD, Mishina Y, Sun H. Bone morphogenetic protein signaling through ACVR1 and BMPRI1A
822 negatively regulates bone mass along with alterations in bone composition. *J Struct Biol*.

2018;201(3):237-46. Epub 2017/11/28. doi: 10.1016/j.jsb.2017.11.010. PubMed PMID: 29175363; PMCID: PMC5820174.

69. Dempster DW, Compston JE, Drezner MK, Glorieux FH, Kanis JA, Malluche H, Meunier PJ, Ott SM, Recker RR, Parfitt AM. Standardized nomenclature, symbols, and units for bone histomorphometry: a 2012 update of the report of the ASBMR Histomorphometry Nomenclature Committee. J Bone Miner Res. 2013;28(1):2-17. Epub 2012/12/01. doi: 10.1002/jbmr.1805. PubMed PMID: 23197339; PMCID: PMC3672237.

70. Chen K, Ng PY, Chen R, Hu D, Berry S, Baron R, Gori F. Sfrp4 repression of the Ror2/Jnk cascade in osteoclasts protects cortical bone from excessive endosteal resorption. Proc Natl Acad Sci U S A. 2019;116(28):14138-43. Epub 2019/06/27. doi: 10.1073/pnas.1900881116. . PubMed PMID: 31239337; PMCID: PMC6628642.

71. Livak KJ, Schmittgen TD. Analysis of relative gene expression data using real-time quantitative PCR and the 2⁻($\Delta\Delta C_T$) Method. Methods. 2001;25(4):402-8. doi: 10.1006/meth.2001.1262. PubMed PMID: 11846609.

Figure Legends

Figure 1. Skeletal phenotype of mice with *Rspo3* haplo-insufficiency. **a)** *Rspo3* expression in marrow depleted long bones, isolated from WT and *Rspo3*^{+/-} mice (n=4-5). Data show all samples and are the mean \pm SEM **p<0.005 by unpaired Student T-test. **b)** Histomorphometric analysis in 6-, 12- and 18-wk males and females (red line=WT, black line=*Rspo3*^{+/-}). (n=3-9). Data are the mean \pm SEM. Two-Way ANOVA followed by Fisher's LSD test. *p<0.05, **p<0.005, ****p<0.0001. **c)** Representative images of Von Kossa staining in 12 wk-old WT and *Rspo3*^{+/-} male tibiae. **d)** Histomorphometric analysis of 12 wk-old WT and *Rspo3*^{+/-} female and male tibiae (n=3-9). Data show all samples and the mean \pm SEM. *p<0.05, **p<0.005 by unpaired Student T-test. Red circles=WT, Black circles=*Rspo3*^{+/-}. **e)** Representative images of double labelling in trabecular bone in 12 wk-old WT and *Rspo3*^{+/-} male tibiae.

849 **Figure 2.** *Rspo3* haplo-insufficiency increases the % of osteoprogenitors. **a)** Representative images
850 of Flow cytometry analysis. **b)** Quantification of the % of Lin⁻Cd45⁻Cd31⁻CD51⁺Sca⁺ cells in WT and
851 *Rspo3*^{+/-} bone marrow. Data show all samples and the mean±SEM (n=10) *=p<0.05 by unpaired
852 Student T-test. **c)** Representative images of CFU-F and CFU-OB assay and quantification in WT and
853 *Rspo3*^{+/-} mice treated in the absence and presence of *Rspo3*. Data show all samples and the
854 mean±SEM (n=4-9) *=p<0.05, **=p<0.005 by Two-Way ANOVA followed by Fisher's LSD test.

855 **Figure 3.** Appendicular skeletal phenotype of mice with *Rspo3* targeted deletion in Runx2⁺ cells
856 (*Rspo3*-OB-cKO). **a)** *Rspo3* expression in marrow depleted long bones, showing deletion efficiency
857 (n=6-7). Data show all samples and are the mean±SEM. **p=0.0019 by unpaired Student T-test. **b)**
858 Representative images of Von Kossa staining in 8-wk old *Rspo3*^{fl} and *Rspo3*-OB-cKO tibiae. **c)**
859 BV/TV, MAR, BFR/BS and N.Ob/BPm by histomorphometric analysis in *Rspo3*^{fl} and *Rspo3*-OB-cKO
860 females and males (n= 7-10). **d)** Structural parameters by µCT analysis *Rspo3*^{fl} and *Rspo3*-OB-cKO
861 femur (n= 6-7). Data show all samples and the mean±SEM *=p<0.05, **=p<0.005, ****=p<0.0001
862 compared to the correspondent *Rspo3*^{fl} group by unpaired Student T-test. Open circles=*Rspo3*^{fl} and
863 filled circles= *Rspo3*-OB-cKO.

864 **Figure 4.** Axial skeletal phenotype of mice with *Rspo3* targeted deletion in Runx2⁺ cells (*Rspo3*-OB-
865 cKO). **a)** *Rspo3* expression in vertebrae, showing deletion efficiency (n=3-5). Data show all samples
866 and are the mean±SEM **p=0.005 by unpaired Student T-test. **b)** Structural parameters by µCT
867 analysis *Rspo3*^{fl} and *Rspo3*-OB-cKO L5 vertebrae (n= 7-10). **c)** Representative images of Von Kossa
868 staining in 8-wk old *Rspo3*^{fl} and *Rspo3*-OB-cKO L5 vertebrae. **d)** BV/TV, Tb.N, MAR, BFR/BS,
869 N.OC/BPm and N.Ob/BPm by histomorphometric analysis in *Rspo3*^{fl} and *Rspo3*-OB-cKO females
870 and males (n= 7-10). Data show all samples and the mean±SEM *=p<0.05, **=p<0.005,
871 ****=p<0.0001 compared to the correspondent *Rspo3*^{fl} group by unpaired Student T-test. Open circles
872 = *Rspo3*^{fl} and filled circles = *Rspo3*-OB-cKO.

873 **Figure 5.** *Rspo3* haplo-insufficiency leads to Wnt signaling activation. **a)** Expression of *Rspo3*,
874 *Runx2* and selected Wnt target genes in BMSCs (n=3-4). Data show all samples and the mean \pm SEM.
875 **b)** Representative images and quantification of active β -catenin by Western analysis in BMSC
876 isolated from WT and *Rspo3*^{+/-} mice (n=7). **c)** Expression of selected Wnt target genes in marrow
877 depleted long bones (n=3-7). Data show all samples and the mean \pm SEM. *p<0.05, **p<0.005,
878 ***p<0.0005 by unpaired Student T-test.

879 **Figure 6.** *Rspo3* deletion leads to Wnt signaling activation *in vitro*. **a)** Luciferase assay and Wnt
880 target gene expression in WT and *Rspo*^{-/-} MEFs treated w/wo Wnt3a (n=6-11). Data show all samples
881 and the mean \pm SEM. **b)** Representative images and quantification of active β -catenin, pLrp6 and Tcf1
882 by Western analysis in WT and *Rspo*^{-/-} MEFs treated w/wo Wnt3a (n=3-7). Data show all samples and
883 the mean \pm SEM. a=p<0.05 vs vehicle WT, b=p<0.05 vs Wnt3a-treated WT and c= p<0.05 vs Wnt3a
884 treated *Rspo3*^{-/-} by Two-Way ANOVA followed by Fisher's LSD test.

885 **Figure 7.** *Rspo3* deletion/ haplo-insufficiency impairs Dkk1 efficacy. **a)** Regulation of *Rspo3* by Wnt3a
886 and Dkk1 in WT MEFs (n=3) Data are the mean \pm SEM. ***p<0.0005, ****p<0.0001, by Student-t test.
887 **b)** Luciferase assay in WT and *Rspo*^{-/-} MEFs treated w/wo Wnt3a and increasing doses of Dkk1 (n=3-
888 4). Data are the mean \pm SEM **p<0.005, ***p<0.0005 compared to vehicle same genotype by
889 unpaired Student-t test. **c)** Representative images and quantification of active β -catenin and pLrp6 by
890 Western analysis in WT and *Rspo3*^{-/-} MEFs treated w/wo Wnt3a and increasing doses of Dkk1 (n=3).
891 Data are the mean \pm SEM *p<0.05, **p,0.005 vs WT vehicle, # p<0.05, vs Wnt3a-treated same
892 genotype by unpaired Student-t test. **d)** Representative images of Von Kossa staining in 6-wk old
893 female mice. **e)** BV/TV, MAR, BFR/BS and N.Ob./B.pm by histomorphometric analysis in females (n=
894 5-6). Data show all samples and the mean \pm SEM a=p<0.05 compared to *control* mice, b= p<0.05
895 compared to *Rspo3*^{+/-} mice, c=p<0.05 compared to *Dkk1-Tg* mice by Two-Way ANOVA followed by
896 Fisher's LSD test.

Figure 8. Erk signaling is involved in the Wnt signaling activation seen in the absence of Rspo3. **a)** Representative images and quantification of pERK, active β -catenin and pLrp6 levels by western analysis in WT and *Rspo3*^{-/-} MEFs treated w/wo Wnt3a and U0126. **b)** Expression of Wnt target genes in WT and *Rspo3*^{-/-} MEFs treated w/wo Wnt3a and U0126. Data show all samples and the mean \pm SEM (n=3-4) *p<0.05, **p<0.005 vs vehicle of the same genotype, ^ = p<0.05 vs WT vehicle and # p<0.05 vs Wnt3a-treated same genotype by unpaired Student-t test.

Figure 9. Effect of Erk signaling inhibition of CFU assays. Representative images of CFU-F and CFU-OB and quantification in WT and *Rspo3*^{+/-} mice treated with and w/o U0126. Data show all samples and the mean \pm SEM (n=3) *=p<0.05, **=p<0.005, ****=p<0.0001 Two-Way ANOVA followed by Fisher's LSD test.

Figure 10. Proposed model. Rspo3 has a dual mode of action to regulate canonical Wnt signaling and thereby bone formation. This duality is based on the regulation of two distinct signaling cascades and their crosstalk: Rspo3 functions via both the Lgr/Rnf43/Znrf3 and the Lgr/Erk axes. In the presence of Rspo3, the Rspo3/Lgr/Rnf43/Znrf3 axis boosts Wnt signaling strengths by the membrane clearance of Rnf43/Znrf3 and subsequent stabilization of Fzd receptors. In addition, binding of Rspo3 to Lgr impairs Erk signaling likely due to the membrane clearance of the Lgr/Rnf43/Znrf3 receptors, preventing Erk signaling activation. Deletion of Rspo3 would dampen Wnt signaling at the cell surface by preventing the Rnf43/Znrf3 effects while promoting Erk activation downstream of Lgr receptors in turn enhancing Lrp5/6 phosphorylation and β -catenin stabilization intracellularly, which has a more potent effect and overcompensates the decrease in Rspo3-dependent proximal Wnt activation in osteoblasts and their progenitors. *Figure created with Biorender.*

Figure 5-source data 1. *Rspo3* haplo-insufficiency leads to Wnt signaling activation. Representative image active β -catenin by Western analysis in BMSC isolated from WT and *Rspo3*^{+/-} mice (n=7).

Figure 5-source data 2. *Rspo3* haplo-insufficiency leads to Wnt signaling activation. Representative image of actin by Western analysis in BMSC isolated from WT and *Rspo3*^{+/-} mice (n=7).

Figure 6-source data 1. *Rspo3* deletion leads to Wnt signaling activation *in vitro*. Representative image of active β -catenin by Western analysis in WT and *Rspo3*^{-/-} MEFs treated w/wo Wnt3a (n=7).

Figure 6-source data 2. *Rspo3* deletion leads to Wnt signaling activation *in vitro*. Representative image of pLrp6 by Western analysis in WT and *Rspo3*^{-/-} MEFs treated w/wo Wnt3a (n=7).

Figure 6-source data 3. *Rspo3* deletion leads to Wnt signaling activation *in vitro*. Representative image of actin by Western analysis in WT and *Rspo3*^{-/-} MEFs treated w/wo Wnt3a (n=7).

Figure 6-source data 4. *Rspo3* deletion leads to Wnt signaling activation *in vitro*. Representative image of Tcf1 by Western analysis in WT and *Rspo3*^{-/-} MEFs treated w/wo Wnt3a (n=3).

Figure 6-source data 5. *Rspo3* deletion leads to Wnt signaling activation *in vitro*. Representative image of Gapdh by Western analysis in WT and *Rspo3*^{-/-} MEFs treated w/wo Wnt3a (n=3).

Figure 7-source data 1-2. *Rspo3* deletion/ haplo-insufficiency impairs Dkk1 efficacy. Representative image of active β -catenin and pLrp6 by Western analysis in WT and *Rspo3*^{-/-} MEFs treated w/wo Wnt3a and increasing doses of Dkk1 (n=3).

Figure 7-source data 3. *Rspo3* deletion/ haplo-insufficiency impairs Dkk1 efficacy. Representative image of actin by Western analysis in WT and *Rspo3*^{-/-} MEFs treated w/wo Wnt3a and increasing doses of Dkk1 (n=3).

Figure 8-source data 1. Erk signaling is involved in the Wnt signaling activation seen in the absence of *Rspo3*. Representative image of active β -catenin in WT and *Rspo3*^{-/-} MEFs treated w/wo w/wo Wnt3a and U0126 (n=3-4).

Figure 8-source data 2. Erk signaling is involved in the Wnt signaling activation seen in the absence of *Rspo3*. Representative image of tubulin levels by western analysis in WT and *Rspo3*^{-/-} MEFs treated w/wo w/wo Wnt3a and U0126 (n=3-4).

Figure 8-source data 3. Erk signaling is involved in the Wnt signaling activation seen in the absence of Rspo3. Representative image of pERK levels by western analysis in WT and *Rspo3*^{-/-} MEFs treated w/wo Wnt3a and U0126 (n=3-4).

Figure 8-source data 4. Erk signaling is involved in the Wnt signaling activation seen in the absence of Rspo3. Representative image of total ERK levels by western analysis in WT and *Rspo3*^{-/-} MEFs treated w/wo Wnt3a and U0126 (n=3-4).

Figure 8-source data 5. Erk signaling is involved in the Wnt signaling activation seen in the absence of Rspo3. Representative image of pLrp6 levels by western analysis in WT and *Rspo3*^{-/-} MEFs treated w/wo Wnt3a and U0126 (n=3-4).

Figure 8-source data 6. Erk signaling is involved in the Wnt signaling activation seen in the absence of Rspo3. Representative image of total Lrp6 levels by western analysis in WT and *Rspo3*^{-/-} MEFs treated w/wo Wnt3a and U0126 (n=3-4).

Figure 8-source data 7. Erk signaling is involved in the Wnt signaling activation seen in the absence of Rspo3. Representative image of Gapdh levels by western analysis in WT and *Rspo3*^{-/-} MEFs treated w/wo Wnt3a and U0126 (n=3-4).

Figure 1- figure supplement 1. Skeletal phenotype of mice with *Rspo3* haploinsufficiency. a) *Rspo3* expression in calvarial OBs Data show all samples and the mean±SEM (n=8) *p<0.05 compared to WT by unpaired Student T test. b) Representative skeletal preparations of WT and *Rspo3*^{+/-} newborn (n=3-4). c) Representative images of Von Kossa staining of 6- and 18-wk old WT and *Rspo3*^{+/-} males.

Figure 1- figure supplement 2. Axial skeletal phenotype of *Rspo3*^{+/-} mice. a) Representative images of Von Kossa staining in 12-wk old WT and *Rspo3*^{+/-} L5 vertebrae. b) Structural parameters by µCT analysis of WT and *Rspo3*^{+/-} females and males (n= 7-9). c) BV/TV, Tb.N, MAR, BFR/BS, N.OC/BPm and N.Ob/BPm by histomorphometric analysis in WT and *Rspo3*^{+/-} females and males (n= 6-7). Data show all samples and the mean±SEM. Red circles= WT and black circles=*Rspo3*^{+/-}.

Figure 1- figure supplement 3. *Rspo3* haploinsufficiency does not affect osteoclastogenesis. a) *Rspo3* expression in BMM-derived osteoclasts. b) Representative images of TRAP staining of WT and *Rspo3*^{+/-} BMM-derived osteoclasts. c) *Nfatc1*, *Trap* and *Ctsk* expression in WT and *Rspo3*^{+/-} BMM-derived osteoclasts. d) Representative mix-matched experiment and quantification of TRAP⁺ BMM-derived osteoclast. Data show all samples and the mean±SEM (n=3) **p=0.0019 by unpaired Student T test.

Figure 3 and 4 – figure supplement 1. Axial (L5) and appendicular (femur) skeletal phenotype of *Runx2-Cre*, WT and *Rspo3*^{fl} mice. a) Structural parameters by µCT analysis at 12 weeks of age (n=3-6). Data show all samples and the mean±SEM. square=*Runx2-Cre*, triangle=WT and black circles=*Rspo3*^{fl}.

Figure 6 – figure supplement 1. Wnt3a and *Rspo3* treatment in WT MEFs. a) Luciferase assay in WT MEFs treated w/wo Wnt3a and *Rspo3* (n=6-7). Data show all samples and the mean±SEM, a=p<0.05 vs vehicle WT, b=p<0.05 vs *Rspo3* treated WT and c= p<0.05 vs Wnt3a treated WT by Two-Way ANOVA followed by Fisher's LSD test. b) Expression of *Rspo3* in WT and *Rspo3*^{+/-} MEFS (n=7). Data show all samples and the mean±SEM. ****p<0.0001 by unpaired Student T-test.

Table S1. Histomorphometric analysis of WT and *Rspo3*^{+/-} males.

Table S2. Histomorphometric analysis of 12 wk-old WT and *Rspo3*^{+/-} vertebrae.

Table S3. Histomorphometric analysis of the tibia midshaft in 12 wk-old WT and *Rspo3*^{+/-} males.

Table S4. Histomorphometric analysis of the tibia midshaft in 12 wk-old WT and *Rspo3*^{+/-} females.

Table S5. Histomorphometric analysis of 8 wk-old *Rspo3*^{fl} and *Rspo3*-OB-cKO mice.

Table S6. Histomorphometric analysis of 8 wk-old *Rspo3*^{fl} and *Rspo3*-OB-cKO vertebrae.

Table S7. Histomorphometric analysis of *Control*, *Rspo3*^{+/-}; *Dkk1-Tg* and *Rspo3*^{+/-}; *Dkk1-Tg* female mice at 6 wk of age.

Acknowledgments

000 This work was supported by NIH-NIAMS R01AR064724 to R.B and in part by NIH-NIDCR
 001 R01DE029615 to F.G.

002 Competing interest statements

003 The Authors do not have competing interest.

004

005

006

007

008

009

010

011

012

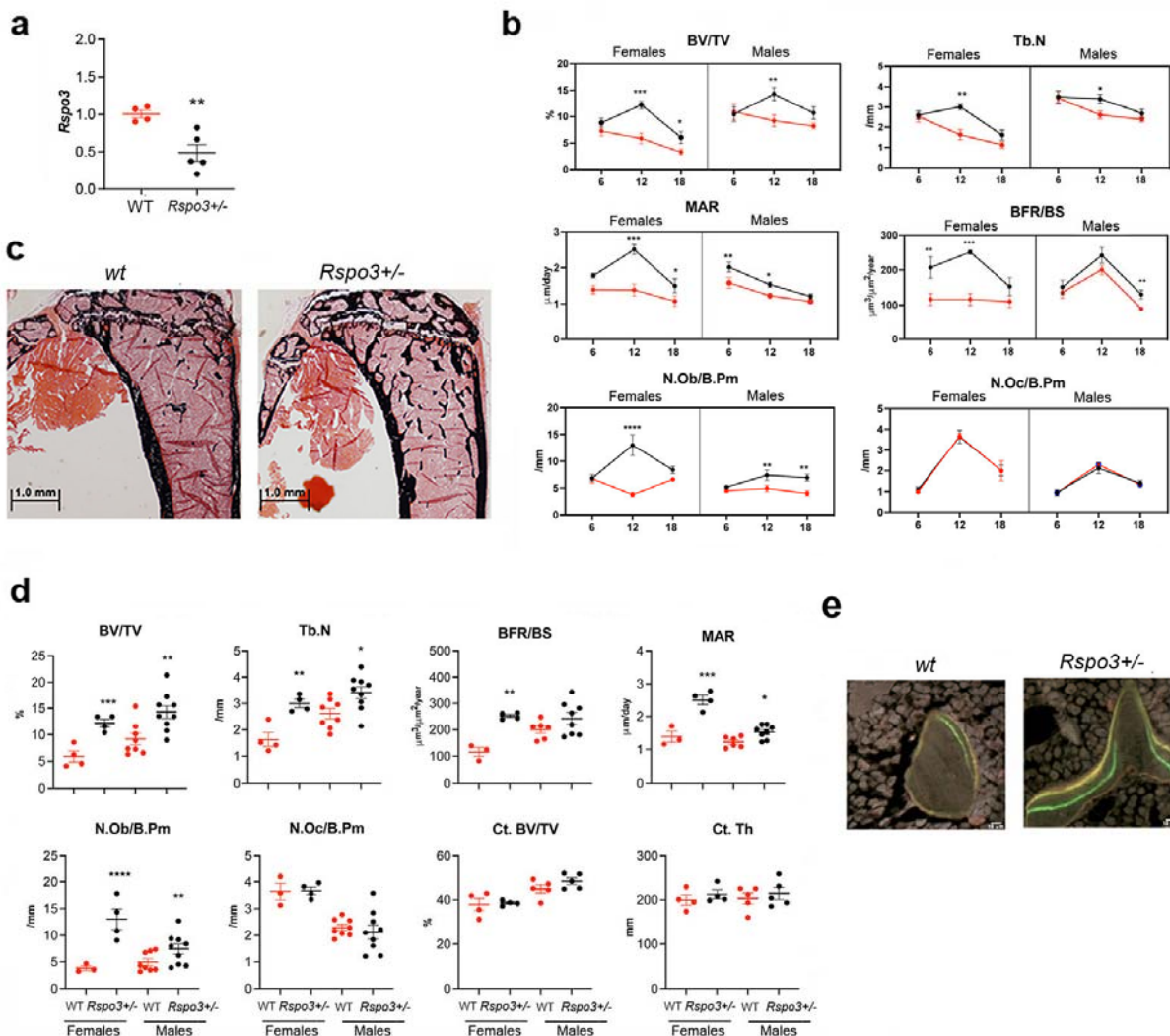


Figure 1. Skeletal phenotype of mice with *Rspo3* haplo-insufficiency. **a)** *Rspo3* expression in marrow depleted long bones, isolated from WT and *Rspo3*^{+/-} mice (n=4-5). Data show all samples and are the mean±SEM **p<0.005 by unpaired Student T-test. **b)** Histomorphometric analysis in 6-, 12- and 18-wk males and females (red line=WT, black line=*Rspo3*^{+/-}). (n=3-9). Data are the mean±SEM. Two-Way ANOVA followed by Fisher's LSD test. *p<0.05, **p<0.005, ****p<0.0001. **c)** Representative images of Von Kossa staining in 12 wk-old WT and *Rspo3*^{+/-} male tibiae. **d)** Histomorphometric analysis of 12 wk-old WT and *Rspo3*^{+/-} female and male tibiae (n=3-9). Data show all samples and the mean ± SEM. *=p<0.05, **p<0.005 by unpaired Student T-test. Red circles=WT, Black circles=*Rspo3*^{+/-}. **e)** Representative images of double labelling in trabecular bone in 12 wk-old WT and *Rspo3*^{+/-} male tibiae.

Table 1. Histomorphometric analysis of WT and *Rspo3*^{+/-} females.

Parameters	6 wk		12 wk		18 wk		Two Way ANOVA		
	WT (n=6)	<i>Rspo3</i> ^{+/-} (n=7)	WT (n=4)	<i>Rspo3</i> ^{+/-} (n=4)	WT (n=8)	<i>Rspo3</i> ^{+/-} (n=6)	Genotype	Age	Interaction
BV/TV (%)	7.24±0.98	8.8±0.88	5.84±1.01	12.2±0.72***	3.28±0.51	6.06±1.1*	<0.0001	<0.0001	NS
Tb.Th (μm)	28.3±0.91	33.6±1.5*	35.8±2.54	40.7±1.31	28.2±1.55	36.8±2.7**	0.0003	0.0032	NS
Tb.N (/mm)	2.53±0.27	2.6±0.20	1.63±0.26	3.00±0.15**	1.13±0.16	1.61±0.25	0.0025	<0.0001	0.0429
Tb.Sp (μm)	397±52.6	368±26.4	618±86.8	297±17.1*	1050±192	690±133	0.0378	0.0008	NS
MAR (μm/day)	1.4±0.11	1.8±0.06	1.39±0.17	2.5±0.14***	1.08±0.15	1.5±0.20*	<0.0001	0.0016	NS
MS/BS (%)	22.2±2.06	31.4±4.05*	23.0±3.25	27.8±1.63	26.8±1.90	27.3±1.55	0.0394	NS	NS
BFR/BS (μm ³ /μm ² /year)	116.2±16.6	207±30.4**	116±16.9	251±6.43**	110±17.6	153±25.1	<0.0001	NS	NS
N.Ob/B.Pm (/mm)	6.72±0.79	6.85±0.64	3.83±0.45	13±1.94****	6.60±0.39	8.4±0.69	<0.0001	NS	0.0001
Ob.S/B.Pm (%)	10.3±1.20	10.5±1.44	4.89±0.38	16.3±2.2****	9.66±0.52	12.3±0.53	<0.0001	NS	0.0007
OS/BS (%)	4.68±0.78	5.51±1.23	2.51±0.30	9.17±0.77***	4.84±0.66	8.3±0.74**	<0.0001	NS	0.0263
O.Th (μm)	3.89±0.30	4.64±0.37	2.76±0.13	4.36±0.09*	2.78±0.37	4.24±0.3**	0.0003	NS	NS
N.Oc/B.Pm (/mm)	1.08±0.13	0.99±0.11	3.64±0.31	3.67±0.14	2.01±0.26	2±0.48	NS	<0.0001	NS
Oc.S/B.Pm (%)	2.98±0.40	3.07±0.37	7.89±0.42	8.77±0.55	5.85±0.86	5.7±1.17	NS	<0.0001	NS
ES/BS (%)	4.41±1.06	4.05±0.42	1.67±0.48	2.96±0.43	6.85±0.82	6.74±1.28	NS	<0.0001	NS

Data are expressed as Mean±SEM. Two Way ANOVA followed by Fisher's LSD post-hoc test.

*=p<0.05, **=p<0.005, ***=p<0.001, ****=p<0.0001 compared to age-matched WT females.

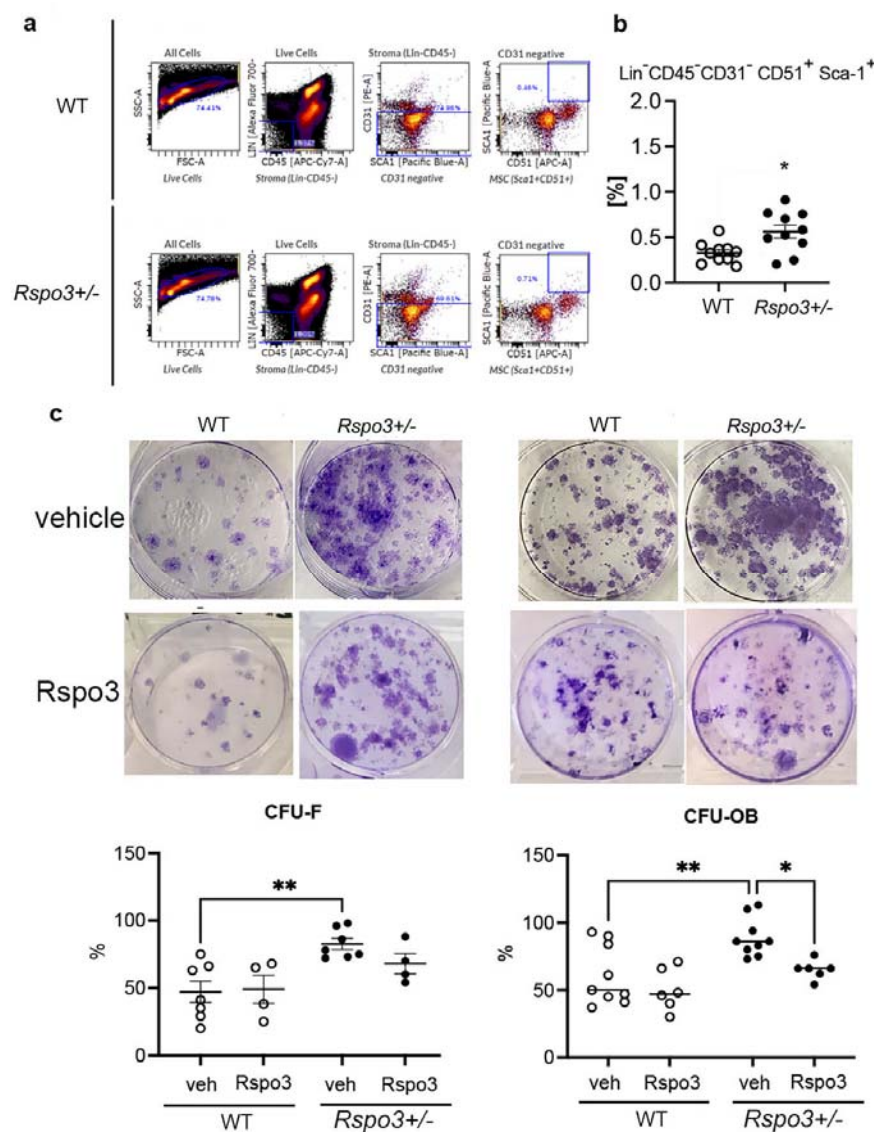


Figure 2. *Rspo3* haplo-insufficiency increases the % of osteoprogenitors. **a**) Representative images of Flow cytometry analysis. **b**) Quantification of the % of Lin⁻CD45⁻CD31⁻CD51⁺Sca⁺ cells in WT and *Rspo3*^{+/-} bone marrow. Data show all samples and the mean \pm SEM (n=10) * p <0.05 by unpaired Student T-test. **c**) Representative images of CFU-F and CFU-OB assay and quantification in WT and *Rspo3*^{+/-} mice treated in the absence and presence of *Rspo3*. Data show all samples and the mean \pm SEM (n=4-9) * p <0.05, ** p <0.005 by Two-Way ANOVA followed by Fisher's LSD test.

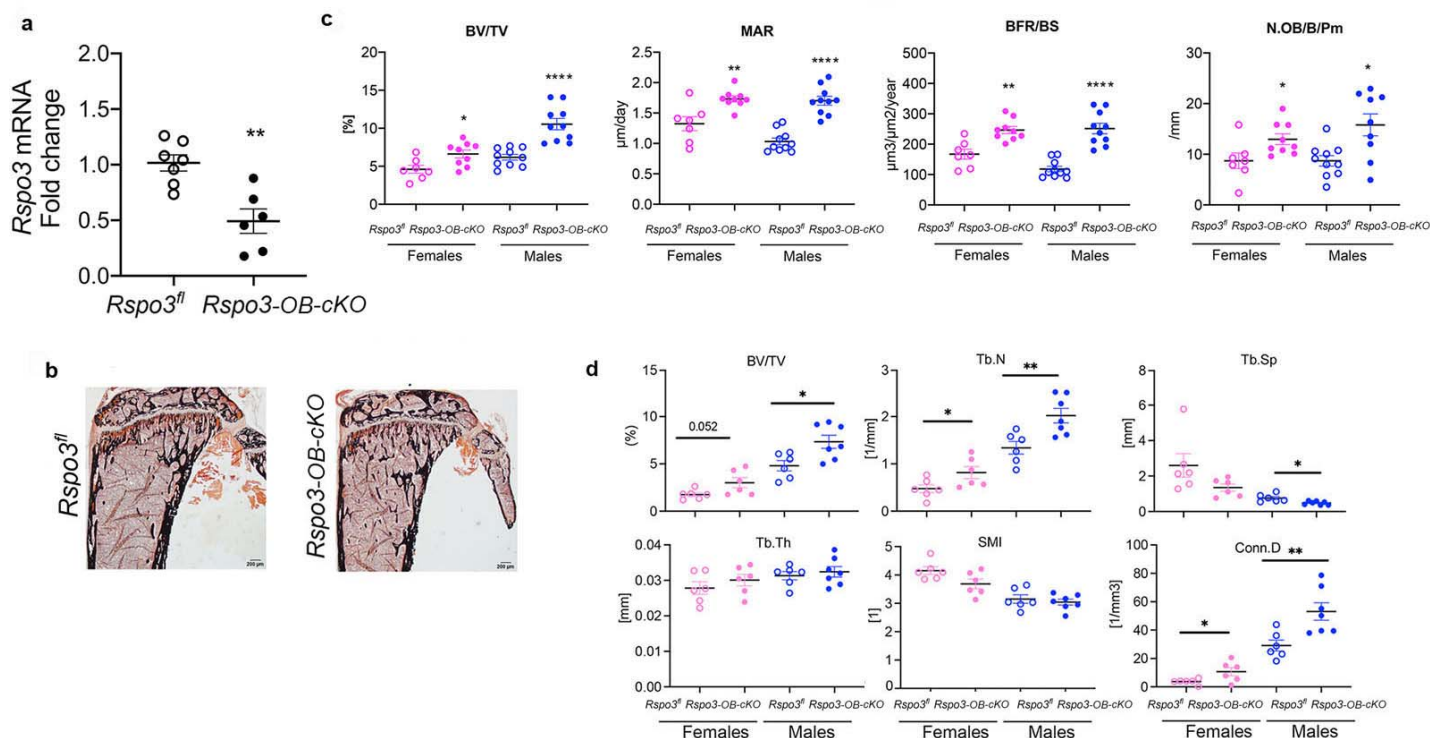


Figure 3. Appendicular skeletal phenotype of mice with *Rspo3* targeted deletion in Runx2⁺ cells (*Rspo3-OB-cKO*). **a** *Rspo3* expression in marrow depleted long bones, showing deletion efficiency (n=6-7). Data show all samples and are the mean±SEM. **p=0.0019 by unpaired Student T-test. **b** Representative images of Von Kossa staining in 8-wk old *Rspo3*^{fl} and *Rspo3-OB-cKO* tibiae. **c** BV/TV, MAR, BFR/BS and N.OB/BPm by histomorphometric analysis in *Rspo3*^{fl} and *Rspo3-OB-cKO* females and males (n= 7-10). **d** Structural parameters by μCT analysis *Rspo3*^{fl} and *Rspo3-OB-cKO* femur (n= 6-7). Data show all samples and the mean±SEM *p<0.05, **p<0.005, ****p<0.0001 compared to the correspondent *Rspo3*^{fl} group by unpaired Student T-test. Open circles=*Rspo3*^{fl} and filled circles= *Rspo3-OB-cKO*.

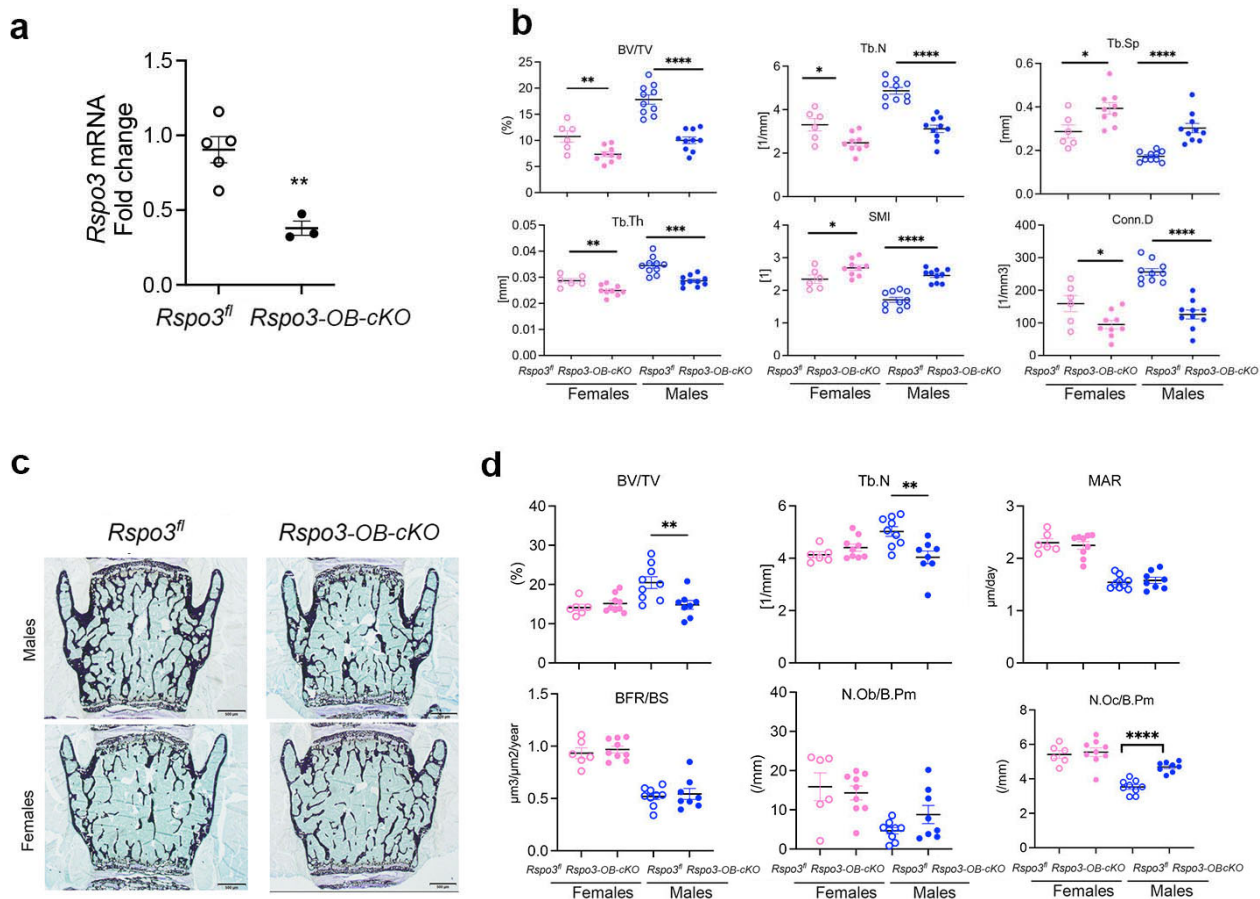


Figure 4. Axial skeletal phenotype of mice with *Rspo3* targeted deletion in Runx2⁺ cells (*Rspo3*-OB-cKO). **a**) *Rspo3* expression in vertebrae, showing deletion efficiency (n=3-5). Data show all samples and are the mean \pm SEM **p=0.005 by unpaired Student T-test. **b**) Structural parameters by μ CT analysis *Rspo3^{fl}* and *Rspo3*-OB-cKO L5 vertebrae (n= 7-10). **c**) Representative images of Von Kossa staining in 8-wk old *Rspo3^{fl}* and *Rspo3*-OB-cKO L5 vertebrae. **d**) BV/TV, Tb.N, MAR, BFR/BS, N.Oc/BPm and N.Ob/BPm by histomorphometric analysis in *Rspo3^{fl}* and *Rspo3*-OB-cKO females and males (n= 7-10). Data show all samples and the mean \pm SEM *p<0.05, **p<0.005, ****=p<0.0001 compared to the correspondent *Rspo3^{fl}* group by unpaired Student T-test. Open circles = *Rspo3^{fl}* and filled circles = *Rspo3*-OB-cKO.

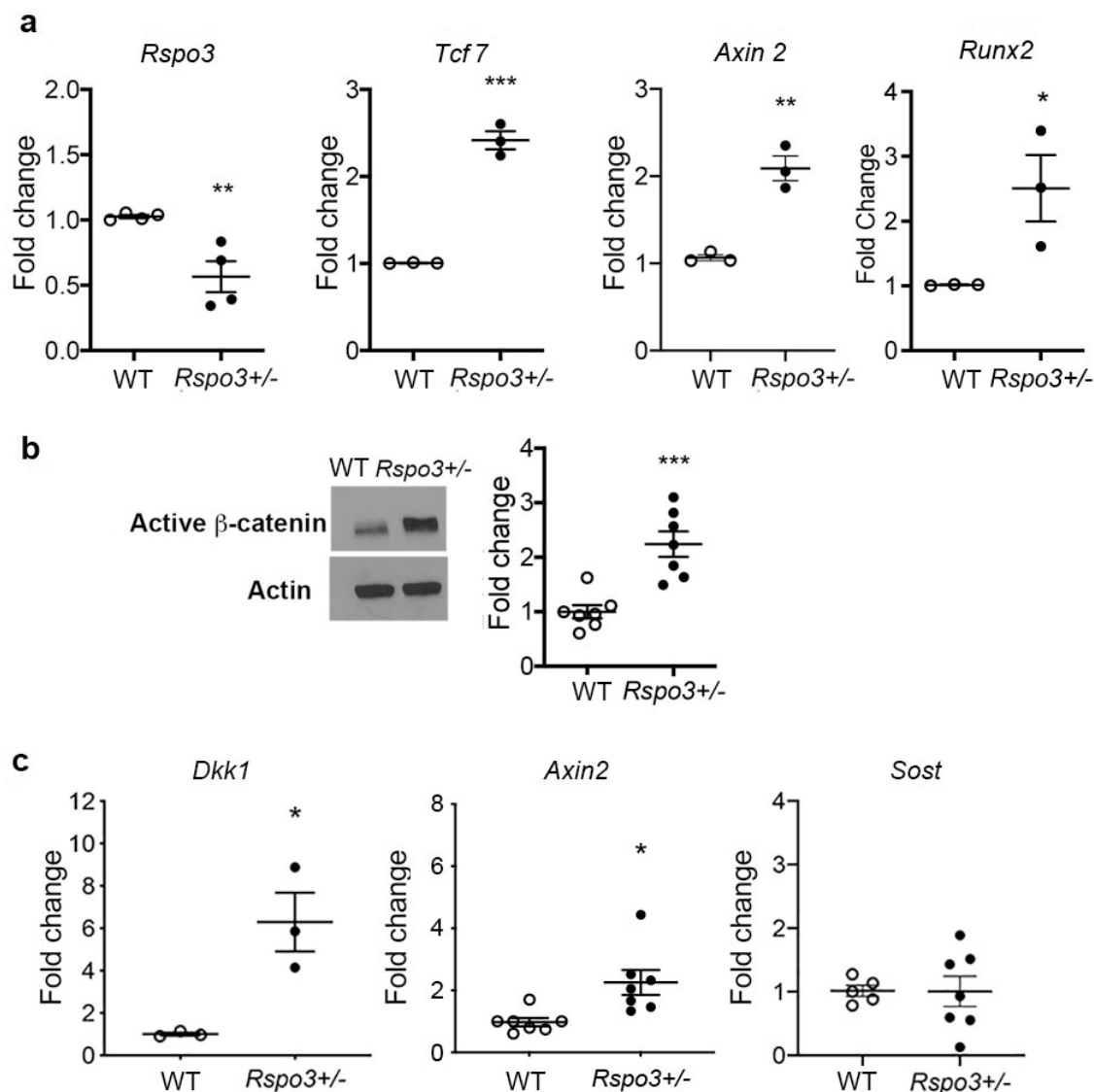


Figure 5. *Rspo3* haplo-insufficiency leads to Wnt signaling activation. **a)** Expression of *Rspo3*, *Runx2* and selected Wnt target genes in BMSCs (n=3-4). Data show all samples and the mean±SEM. **b)** Representative images and quantification of active β-catenin by Western analysis in BMSC isolated from WT and *Rspo3*^{+/-} mice (n=7). **c)** Expression of selected Wnt target genes in marrow depleted long bones (n=3-7). Data show all samples and the mean±SEM. *p<0.05, **p<0.005, ***p<0.0005 by unpaired Student T-test.

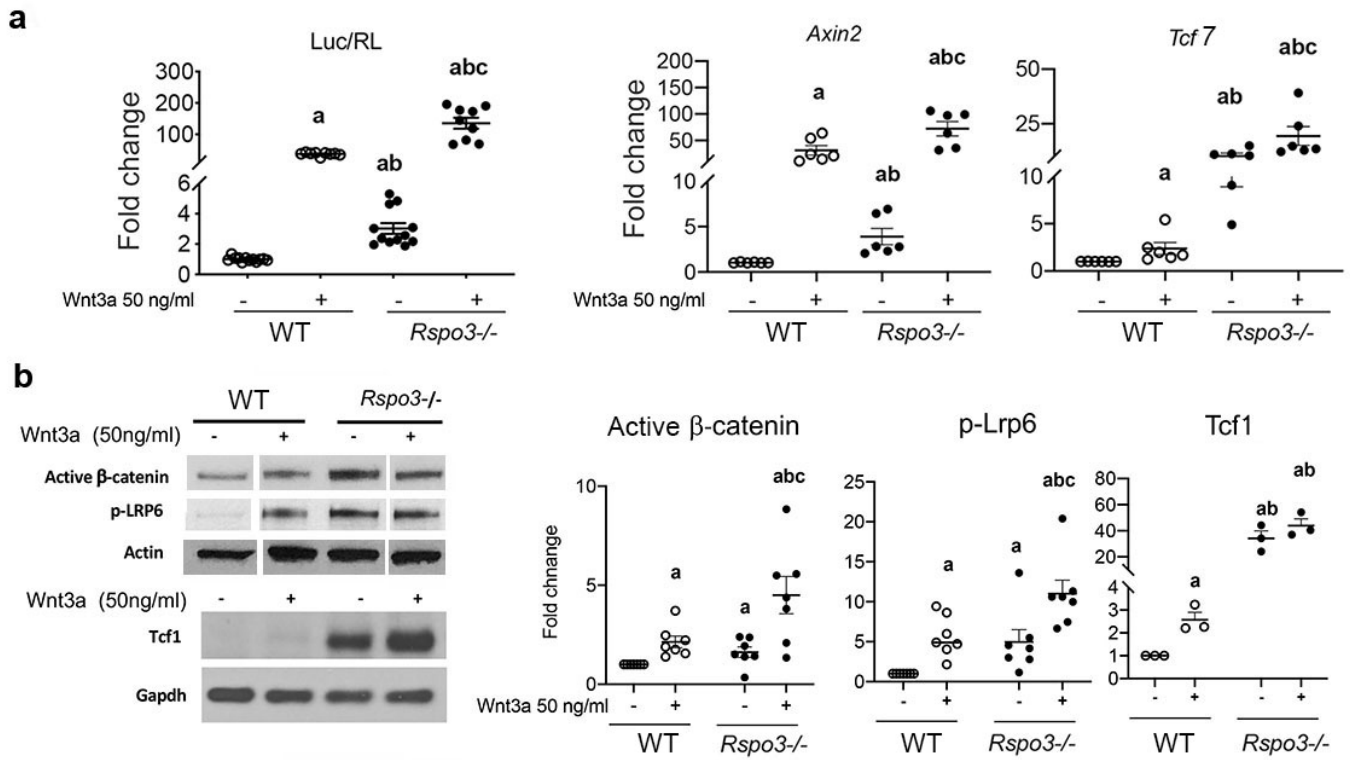


Figure 6. *Rspo3* deletion leads to Wnt signaling activation *in vitro*. **a)** Luciferase assay and Wnt target gene expression in WT and *Rspo3*^{-/-} MEFs treated w/w/o Wnt3a (n=6-11). Data show all samples and the mean±SEM. **b)** Representative images and quantification of active β-catenin, pLrp6 and Tcf1 by Western analysis in WT and *Rspo3*^{-/-} MEFs treated w/w/o Wnt3a (n=3-7). Data show all samples and the mean±SEM. a=p<0.05 vs vehicle WT, b=p<0.05 vs Wnt3a-treated WT and c= p<0.05 vs Wnt3a treated *Rspo3*^{-/-} by Two-Way ANOVA followed by Fisher's LSD test.

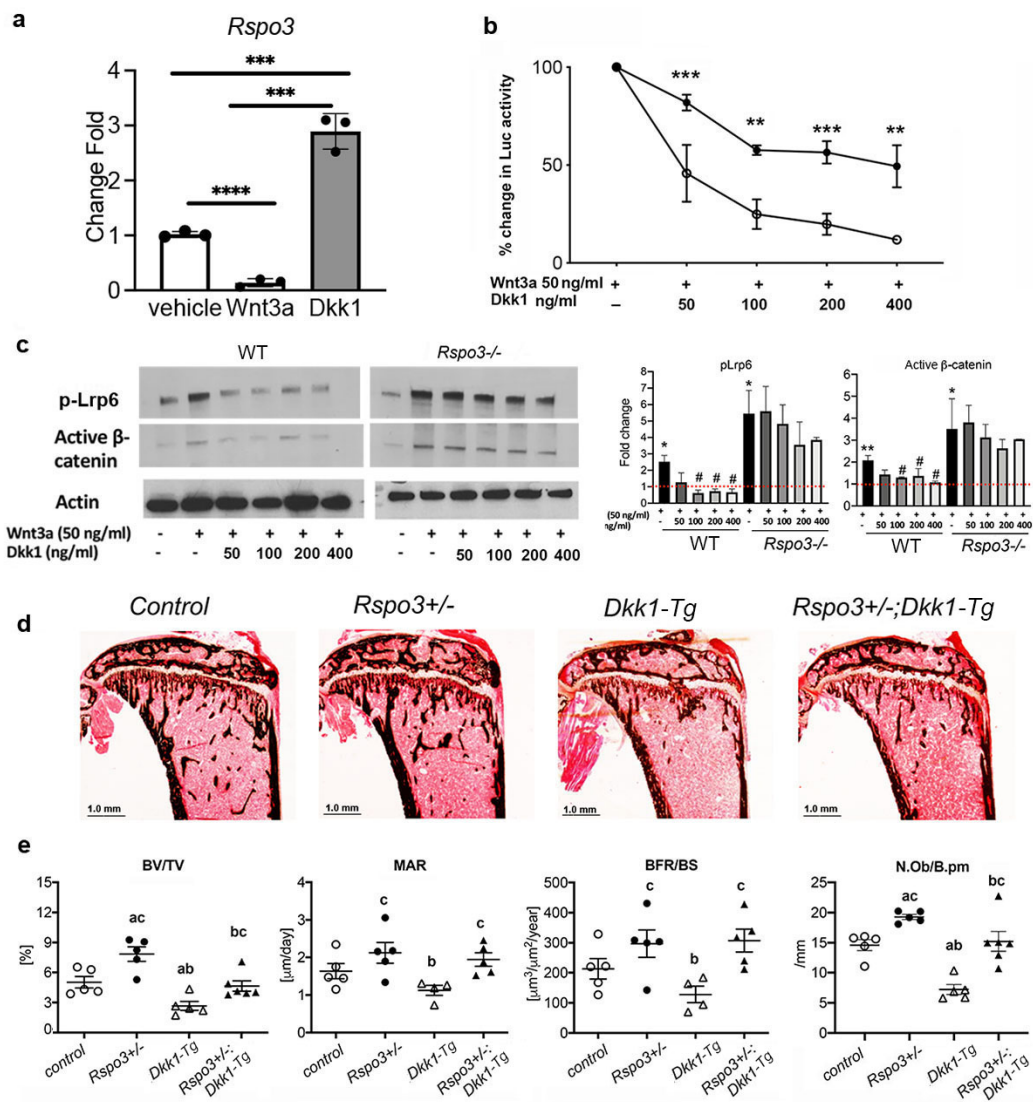


Figure 7. *Rspo3* deletion/ haplo-insufficiency impairs Dkk1 efficacy. **a)** Regulation of *Rspo3* by Wnt3a and Dkk1 in WT MEFs (n=3) Data are the mean±SEM. ***p<0.0005, ****p<0.0001, by Student-t test. **b)** Luciferase assay in WT and *Rspo3*^{-/-} MEFs treated w/wo Wnt3a and increasing doses of Dkk1 (n=3-4). Data are the mean±SEM **p<0.005, ***p<0.0005 compared to vehicle same genotype by unpaired Student-t test. **c)** Representative images and quantification of active β-catenin and pLrp6 by Western analysis in WT and *Rspo3*^{-/-} MEFs treated w/wo Wnt3a and increasing doses of Dkk1 (n=3). Data are the mean ±SEM *p<0.05, **p<0.005 vs WT vehicle, # p<0.05, vs Wnt3a-treated same genotype by unpaired Student-t test. **d)** Representative images of Von Kossa staining in 6-wk old female mice. **e)** BV/TV, MAR, BFR/BS and N.Ob./B.pm by histomorphometric analysis in females (n=

5-6). Data show all samples and the mean \pm SEM a= $p<0.05$ compared to *control* mice, b= $p<0.05$ compared to *Rspo3*^{+/-} mice, c= $p<0.05$ compared to *Dkk1-Tg* mice by Two-Way ANOVA followed by Fisher's LSD test.

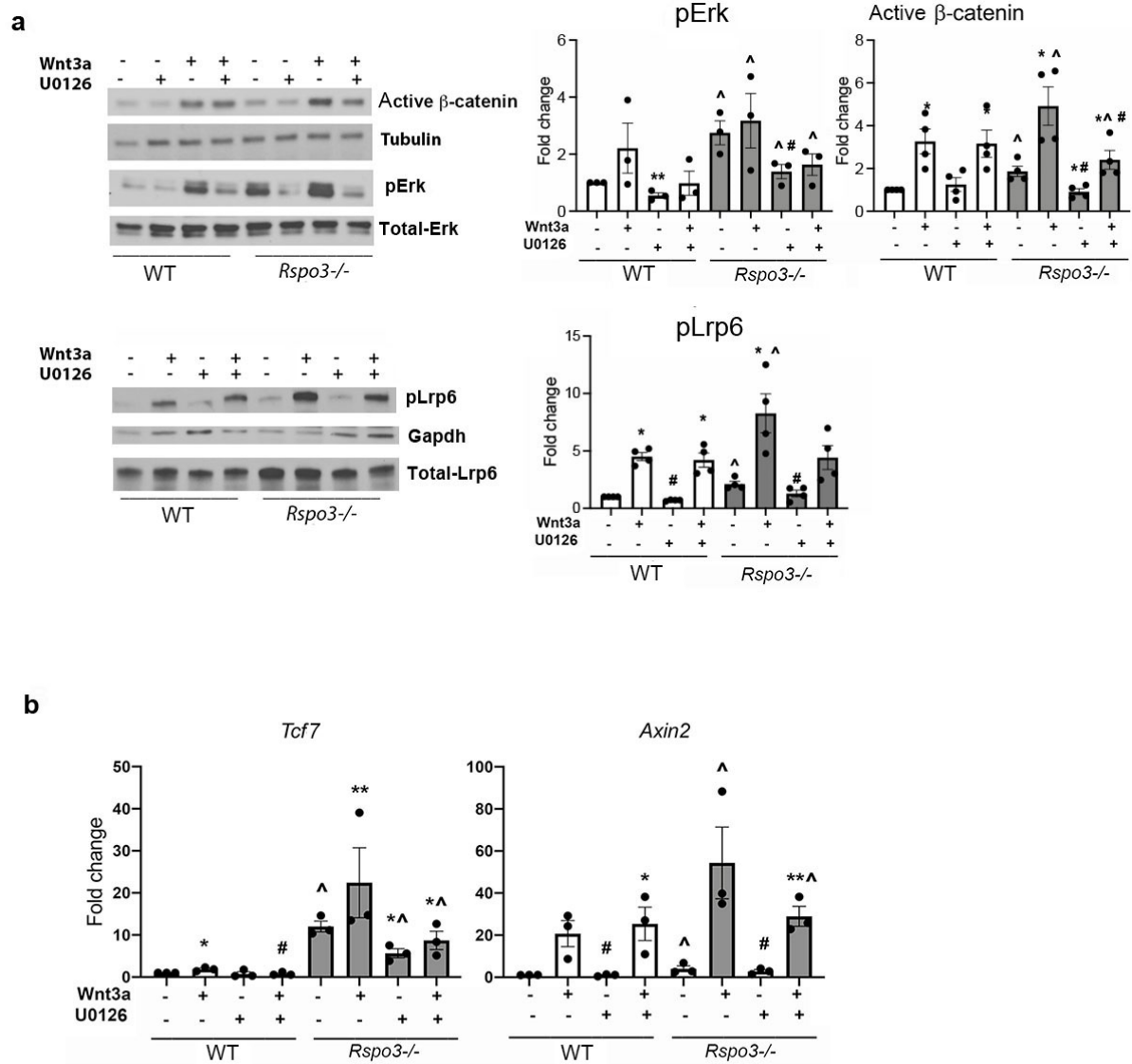


Figure 8. Erk signaling is involved in the Wnt signaling activation seen in the absence of Rspo3. **a)** Representative images and quantification of pERK, active β -catenin and pLrp6 levels by western analysis in WT and *Rspo3*^{-/-} MEFs treated w/wo Wnt3a and U0126. **b)** Expression of Wnt target genes in WT and *Rspo3*^{-/-} MEFs treated w/wo Wnt3a and U0126. Data show all samples and the mean \pm SEM (n=3-4) *p<0.05, **p<0.005 vs vehicle of the same genotype, ^ = p<0.05 vs WT vehicle and # p<0.05 vs Wnt3a-treated same genotype by unpaired Student-t test.

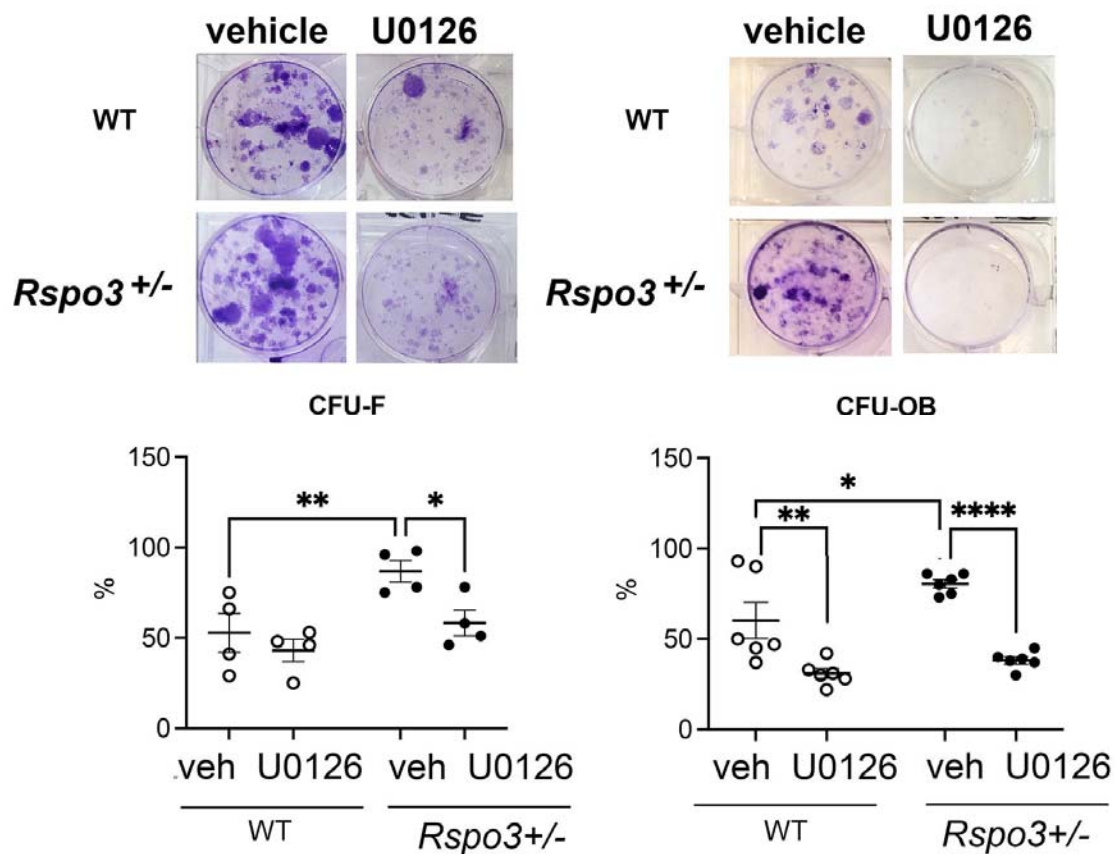


Figure 9. Effect of Erk signaling inhibition of CFU assays. Representative images of CFU-F and CFU-OB and quantification in WT and *Rspo3*^{+/-} mice treated with and w/o U0126. Data show all samples and the mean±SEM (n=3) *=p<0.05, **=p<0.005, ****=p<0.0001 Two-Way ANOVA followed by Fisher's LSD test.

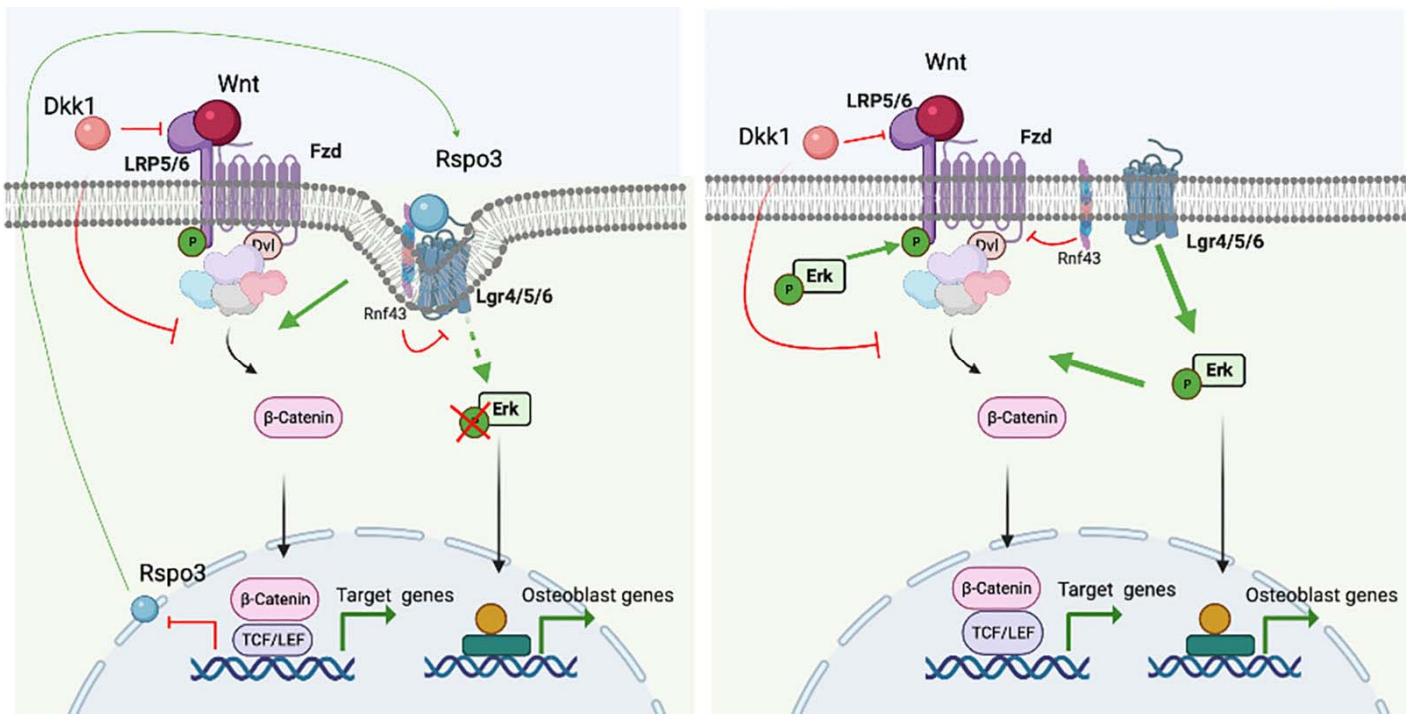


Figure 10. Proposed model. Rspo3 has a dual mode of action to regulate canonical Wnt signaling and thereby bone formation. This duality is based on the regulation of two distinct signaling cascades and their crosstalk: Rspo3 functions via both the Lgr/Rnf43/Znrf3 and the Lgr/Erk axes. In the presence of Rspo3, the Rspo3/Lgr/Rnf43/Znrf3 axis boosts Wnt signaling strengths by the membrane clearance of Rnf43/Znrf3 and subsequent stabilization of Fzd receptors. In addition, binding of Rspo3 to Lgr impairs Erk signaling likely due to the membrane clearance of the Lgr/Rnf43/Znrf3 receptors, preventing Erk signaling activation. Deletion of Rspo3 would dampen Wnt signaling at the cell surface by preventing the Rnf43/Znrf3 effects while promoting Erk activation downstream of Lgr receptors in turn enhancing Lrp5/6 phosphorylation and β-catenin stabilization intracellularly, which has a more potent effect and overcompensates the decrease in Rspo3-dependent proximal Wnt activation in osteoblasts and their progenitors. *Figure created with Biorender.*